THE JOURNAL OF PHYSICAL CHEMISTRY A
A JOURNAL OF THE AMERICAN CHEMICAL SOCIETY

pubs.acs.org/JPCA Article

Directed Gas-Phase Formation of The Propargyl Family of Resonance-Stabilized Radicals in The Reactions of Ground-State Carbon Atoms (C; ^3P_j) with Butene Isomers (C_4H_8): Dimethylpropargyl and Ethylpropargyl

Published as part of The Journal of Physical Chemistry A special issue "Stephen J. Klippenstein Festschrift".

Anatoliy A. Nikolayev, Iakov A. Medvedkov, Surajit Metya, Shane J. Goettl, Alexander M. Mebel,* and Ralf I. Kaiser*

Cite This: *J. Phys. Chem. A* 2026, 130, 4823−4838 Read Online

ACCESS | Metrics & More | Article Recommendations | Supporting Information

ABSTRACT: The propargyl radical (C_3H_3) is the simplest resonance-stabilized free radical (RSFR), but how does stepwise methyl substitution in the alkene reactant affect its dynamics of their formation? We report a crossed molecular beam study of the reactions of atomic carbon (C, ^3P_j) with four butene isomers (C_4H_8) under single-collision conditions at a collision energy of 28 ± 2 kJ mol^{-1}. Barrierless addition of atomic carbon to the alkene C=C bond triggers ring opening to substituted triplet allenes—a *de facto* insertion mechanism—followed by unimolecular decomposition via atomic hydrogen (H), methyl (CH_3), or ethyl (C_2H_5) loss, yielding a family of propargyl-type RSFRs. RRKM calculations reveal that the branching ratios are highly sensitive to the alkene structure. While the methyl loss channel, affording 1-methylpropargyl, dominates for 2-butenes (80−90%), the predicted hydrogen-atom loss channel (≈10%), leading to 1,3-dimethylpropargyl is identified experimentally by comparison with theoretical energetics. For isobutene, near-equal competition is observed, with the reaction producing 3-methylpropargyl (≈50%) and 1,1-dimethylpropargyl (≈40%), along with 2-vinylallyl (≈5%), whose formation is supported by experimental data. Most notably, the reaction with 1-butene uniquely favors an enthalpically driven hydrogen shift, eventually producing 1-vinylallyl (≈38%), which is assigned based on the excellent agreement between the measured and calculated reaction exothermicity. Rapid entropically favored fragmentation channels yield ≈40% of propargyl-type species (propargyl, 1- and 3-ethylpropargyls), slightly outcompeting the allyl-type product. These results establish a systematic progression from C_2H_4 via C_3H_6 to C_4H_8, where the increasing alkyl substitution unlocks new fragmentation channels, providing a versatile gas-phase route to alkylated RSFRs—key intermediates in the growth of methylated and ethylated PAHs and aliphatic chains in combustion and cold interstellar environments (molecular clouds).

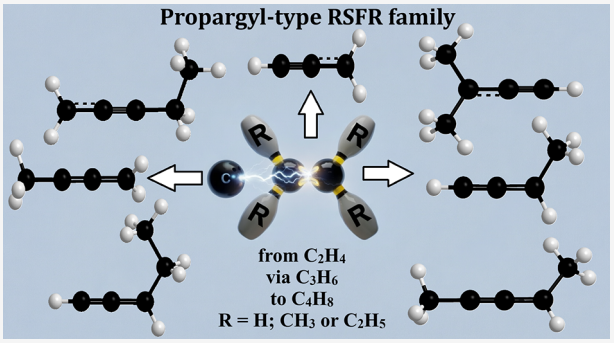

1. INTRODUCTION

As the fourth most abundant element in the universe, ground-state atomic carbon C(^3P_j) has been observed ubiquitously—from interstellar clouds and circumstellar envelopes to planetary atmospheres and plasmas—through its characteristic 609 μm $^3P_1 \rightarrow {}^3P_0$ transition.[1−7] Reactions of atomic carbon with unsaturated hydrocarbons govern molecular growth in both combustion environments and the interstellar medium. In cold molecular clouds, where thermal activation is limited, the electronic structure of C(^3P_j) enables barrierless addition to π-bonded systems, initiating chemical complexity even at cryogenic temperatures.[8−17] A central outcome here is the formation of resonance-stabilized free radicals (RSFRs)—unsaturated, hydrogen-deficient species with delocalized unpaired electrons, resulting in enhanced thermodynamic stability and extended lifetimes. These RSFRs can therefore accumulate and drive molecular mass growth toward increasingly complex hydrocarbons. Among them, the propargyl radical (C_3H_3)—structurally the smallest RSFR—occupies a fundamental position, serving as a versatile building block for both aliphatic chain elongation and the formation

Received: April 28, 2026
Revised: May 27, 2026
Accepted: May 29, 2026
Published: June 12, 2026

https://doi.org/10.1021/acs.jpca.6c02765
J. Phys. Chem. A 2026, 130, 4823−4838

and expansion of aromatic ring systems.[18−26] The pioneering theoretical work of Miller and Klippenstein[18,19] established that propargyl recombination on the C_6H_6 potential energy surface (PES) efficiently yields benzene via third-body stabilization. This reaction scheme was directly validated by Zhao et al.,[22] who identified benzene and fulvene along with a competing phenyl (C_6H_5) plus atomic hydrogen channel in the propargyl radical self-reaction using isomer-selective synchrotron mass spectrometry. Beyond the propargyl self-reaction, the Propargyl Addition-BenzAnnulation (PABA) mechanism[24−26]—propargyl addition to a benzyl moiety followed by hydrogen-assisted benzo- or naphtho-fulvene isomerization—yields naphthalene ($C_{10}H_8$)[24] and larger polycyclic aromatic hydrocarbons (PAHs) such as anthracene/phenanthrene ($C_{14}H_{10}$).[25]

Replacement of propargyl by methyl-substituted propargyl (Schemes 1 and 2) in their self-reactions produces toluene and xylenes, both of which have drawn considerable attention from combustion and astrochemistry communities.[27−39] This demonstrates that even simple RSFR recombination channels contribute to methylated aromatic ring formation. This logic finds a natural extension in the PABA mechanism (Scheme 3), where methyl-substituted propargyl radicals can add to benzyl-type moieties, ultimately yielding methylated PAHs such as methyl-substituted naphthalenes, anthracenes, and phenanthrenes. This is analogous to the Hydrogen Abstraction Vinylacetylene Addition (HAVA) mechanism, where replacement of vinylacetylene by its methyl- and phenyl-substituted counterparts results in methylated and complex aromatics.[40−44] These species are of particular astrochemical relevance, as methylated PAHs have been identified in carbonaceous meteorites.[36,45−52] A key feature of the methyl moiety is its weaker C−H bond compared to aromatic C−H bonds by 100 kJ mol^{-1}.[33,53−57] The methylated PAH formed from methylated propargyls and benzyl- or even xylyl-type radicals can thus easily lose atomic hydrogen from a methyl group, regenerating the benzyl- or xylyl-type radical. This creates a sequence where a smaller RSFR repeatedly adds to a regenerating radical, driving the growth of methylated PAHs.[24,33] In contrast to ring annulation, propargyl can also engage in barrierless reactions that elongate aliphatic chains. A

Scheme 1. Molecular Structure of Substituted Resonantly Stabilized Propargyl Radical

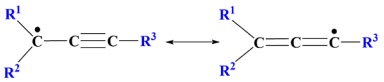

Scheme 2. Self-Reactions of the Propargyl Radical and Its Methyl-Substituted Derivatives Leading to Toluene, Xylenes, and Their Corresponding Aromatic Resonance-Stabilized Free Radicals (RSFRs). The Formation of the Simplest Aromatic Benzyl radical—as Accessed via Photolysis or H-Assisted H-Abstraction—is Shown Here for Illustration

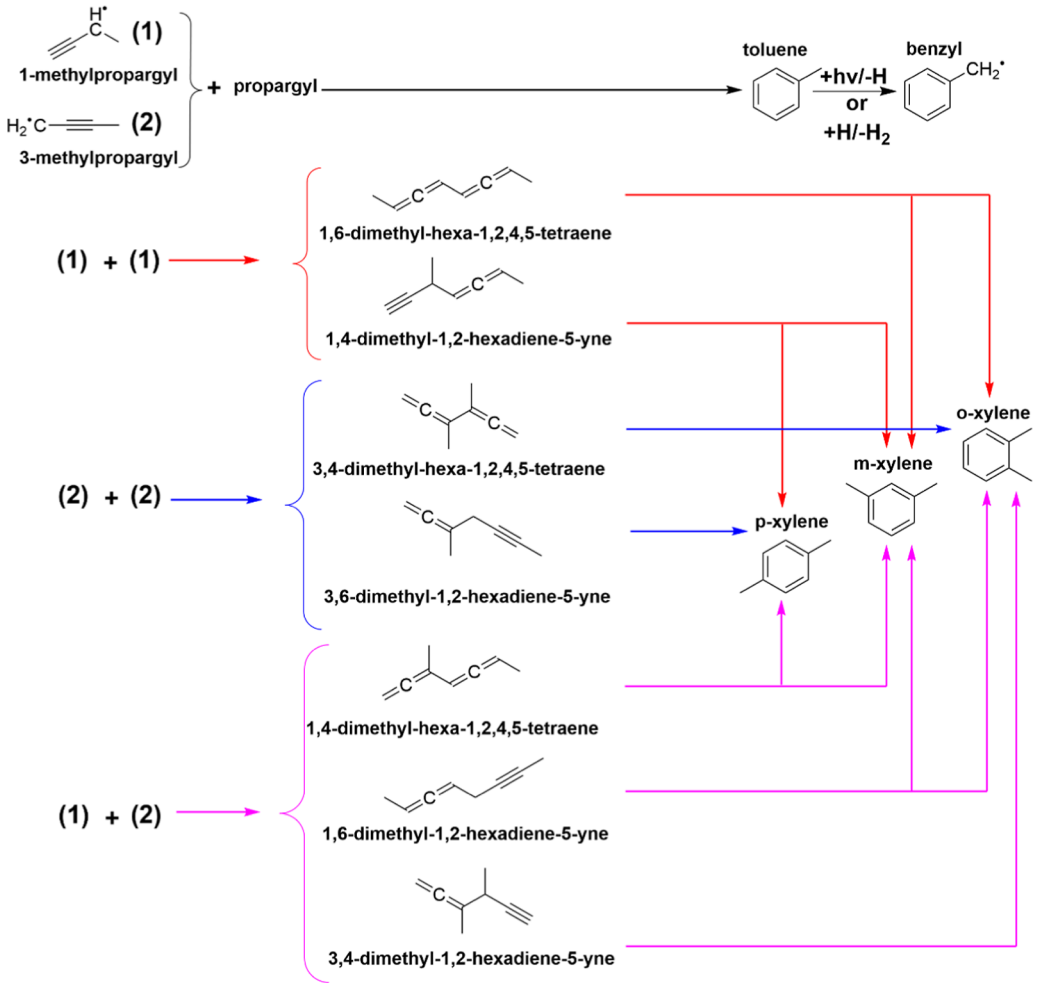

https://doi.org/10.1021/acs.jpca.6c02765
J. Phys. Chem. A 2026, 130, 4823−4838

Scheme 3. Propargyl Addition-BenzAnnulation (PABA) Mechanism Involving Methyl-Substituted Propargyl Radicals

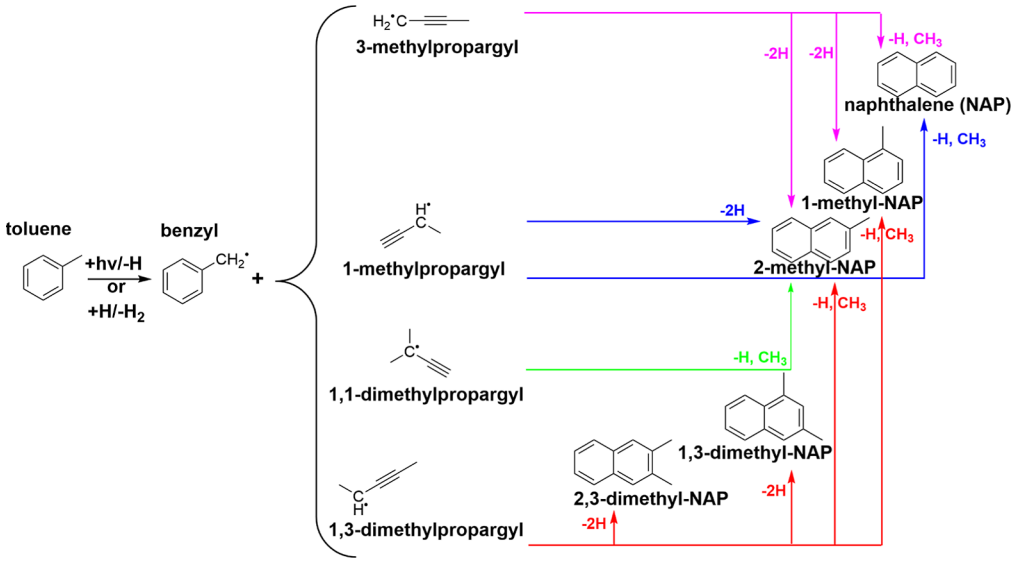

striking example is a gas-phase reaction of propargyl with tricarbon (C_3), a closed-shell carbene, which produces ethynylbutatrienylidene (HCCCHCCC)—a high-energy isomer of triacetylene (C_6H_2).[23] Crucially, this duality extends to methyl-substituted propargyl radicals. When such methylated RSFRs react with tricarbon, the resulting products are expected to be methylated, hydrogen-deficient hydrocarbon chains. Aliphatic chains and their methylated counterparts have been observed in space, and their formation mechanisms are no less significant than those of PAHs.[40,58]

The formation of propargyl and substituted propargyl radicals is also linked to reactions of C(^3P_j) with the smallest unsaturated hydrocarbons. These systems have been extensively investigated under single-collision conditions using crossed molecular beam (CMB) experiments combined with high-level electronic structure calculations, providing detailed insight into reaction dynamics and product branching.[21,59,60] In particular, reactions of C(^3P_j) with ethylene (C_2H_4)[60−65] and propene (C_3H_6)[60,66,67] proceed via barrierless addition to the C═C bond followed by hydrogen or methyl elimination, yielding propargyl and methyl-substituted propargyl radicals, respectively. As a logical next step, the reaction of atomic carbon with four butene (C_4H_8) isomers allows us to probe how the increasing structural complexity impacts RSFR formation and the resulting molecular mass growth. Experimental studies of these systems have primarily relied on bulk methods,[68] such as flow reactor and kinetic measurements, which provide information on overall rate constants and (rarely) product distributions, but do not resolve the underlying reaction dynamics at the single-collision level.

Here, we combine crossed molecular beam experiments with high-level quantum chemical calculations to unravel the reaction dynamics of ground-state atomic carbon (C, ^3P_j) with four C_4H_8 isomers—1-butene (X^1A), *cis*-2-butene (X^1A_1), *trans*-2-butene (X^1A_g), and isobutene (X^1A_1)—under single-collision conditions. These reactions are found to proceed via barrierless addition of the carbon atom to the carbon−carbon double bond, followed by ring opening to substituted triplet allenes and unimolecular decomposition through atomic hydrogen, methyl, or ethyl loss, predominantly yielding RSFRs of the propargyl family.

2. METHODS

2.1. Crossed Molecular Beam Experiment

The gas-phase reactions of atomic carbon (C; ^3P_j) with butene isomers (C_4H_8) were investigated under single-collision conditions using a crossed molecular beams machine.[69,70] The experimental setup, data acquisition, and data processing methodologies have been described in detail previously.[33,71−73] Briefly, a supersonic molecular beam of atomic carbon was generated in situ in the primary source chamber via laser ablation (3 mJ, 266 nm, 30 Hz, Quanta-Ray) of a rotating and translating carbon rod. The ablated species were seeded in a neat carrier gas (He, 99.9999%; Airgas) released by a pulsed valve operating at 60 Hz with a backing pressure of 4 atm. A four-slot chopper wheel, positioned between the skimmer of the primary source and the cold shield, selected a segment of the pulsed carbon beam with a peak velocity of v_p = 2316 ± 51 m s^{-1} and a speed ratio S = 3.6 ± 0.3. These beams intersected perpendicularly in the reaction chamber with pulsed molecular beams of neat butene isomers (1-butene, *cis*-2-butene, *trans*-2-butene, isobutene; Sigma-Aldrich; ≥99%), resulting in a mean collision energy of 28 ± 2 kJ mol^{-1}. The secondary beam was characterized by a peak velocity of v_p = 760 ± 30 m s^{-1} and a speed ratio S = 7 ± 1.

The reactively scattered products were monitored using a triply differentially pumped (10^{-12} Torr) quadrupole mass spectrometric (QMS) detector operated in the time-of-flight (TOF) mode with electron ionization (80 eV, 2 mA).[74−76] This "universal" detector can be rotated within the plane defined by the primary and secondary reactant beams to record angularly resolved TOF spectra. The recorded TOF spectra were integrated and normalized to extract the product laboratory angular distribution (LAD)—the signal intensity of a specific mass-to-charge ratio (m/z) as a function of the laboratory angle. To elucidate the reaction dynamics, the TOF spectra and LAD were transformed from the laboratory frame to the center-of-mass (CM) frame using a forward-convolution routine.[77,78] This method employs trial angular flux $T(\theta)$ and translational energy $P(E_T)$ distributions in the CM frame to simulate the laboratory data. The CM functions were iteratively adjusted until the optimal fit of the TOF spectra and LAD was achieved. Together, these functions constitute the reactive differential cross sections $I(\theta,u) \sim P(u)\times T(\theta)$,[79,80] where u is the CM velocity and θ is the scattering angle in the CM system.

2.2. Computational Methods

All geometry optimizations and vibrational frequency calculations for stationary points—including reactants, products, intermediates, and transition states—on the triplet C_5H_8 potential energy surfaces

https://doi.org/10.1021/acs.jpca.6c02765
J. Phys. Chem. A 2026, 130, 4823−4838

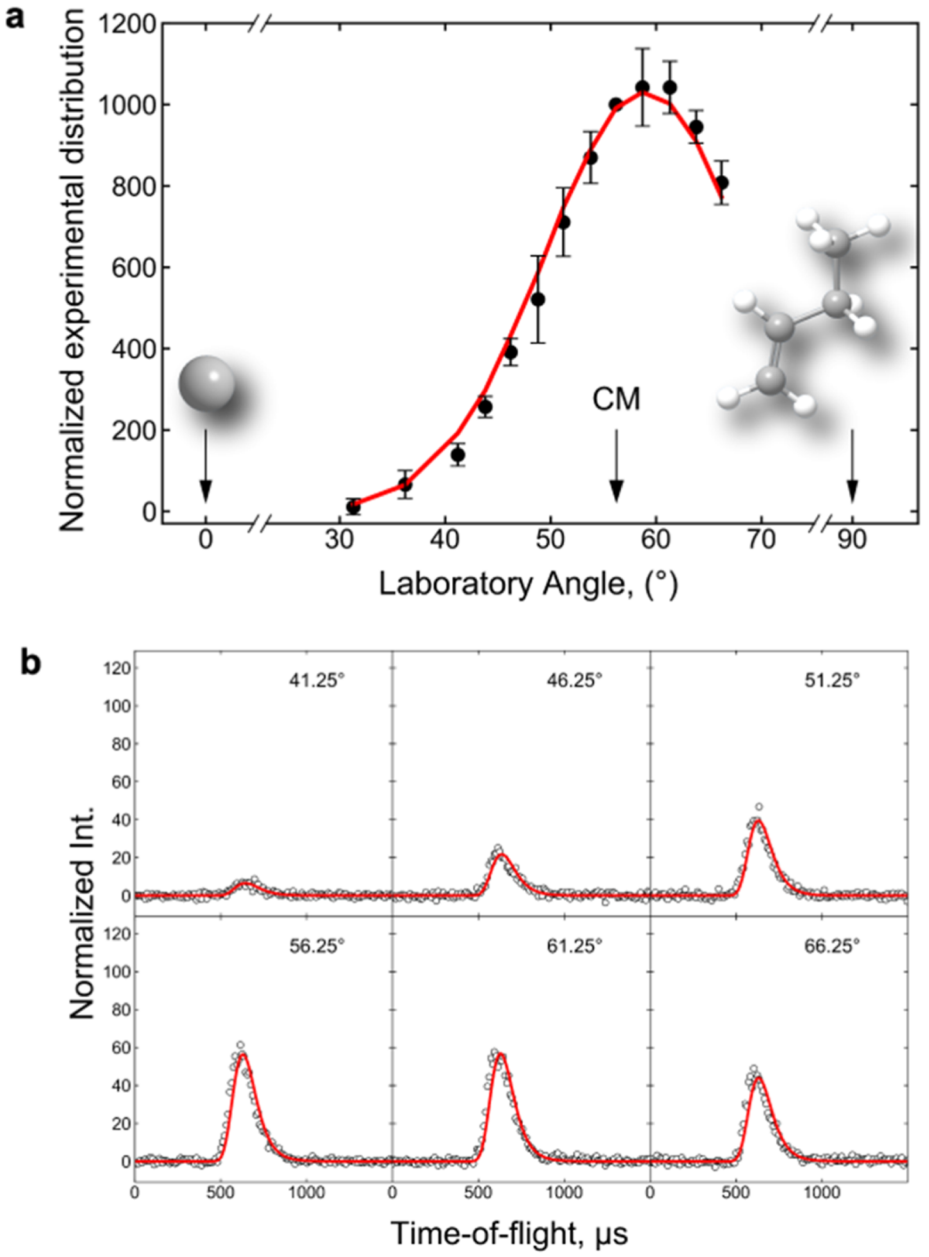

Figure 1. (a) Laboratory angular distribution and (b) time-of-flight (TOF) spectra recorded at $m/z = 66$ for the reaction of atomic carbon (C; ^3P_j) with 1-butene (C_4H_8; X^1A) at a collision energy of 28 ± 2 kJ mol^{-1}. The circles represent the experimental data, and the solid lines indicate the best fits obtained using the forward-convolution routine.

(PESs) accessed by the reactions of the four butene isomers with atomic carbon were carried out using the long-range corrected hybrid ωB97X-D[81] density functional together with Pople's split-valence 6-311G(d,p) basis set[82] as implemented in the Gaussian 09 package.[83] The nature of each transition state was verified through intrinsic reaction coordinate (IRC) calculations[84] at the same ωB97X-D/6-311G(d,p) level. To refine the DFT relative energies, single-point energy calculations were subsequently performed in Molpro 2015[85] using the explicitly correlated restricted open-shell coupled cluster method with single and double excitations and perturbative treatment of triple excitations—RCCSD(T)-F12b[86,87]—in conjunction with Dunning's correlation-consistent triple-ζ cc-pVTZ-f12 basis set.[88] The final relative energies computed using the CCSD(T)-F12/cc-pVTZ-f12//ωB97X-D/6-311G(d,p) + ZPE(ωB97X-D/6-311G(d,p)) protocol are expected to be accurate to within 4 kJ mol^{-1}.[89]

For each of the four butene isomers separately, energy-dependent rate constants for all unimolecular steps on the C_5H_8 PESs were evaluated within the Rice–Ramsperger–Kassel–Marcus (RRKM) framework.[80,90,91] The internal energy of each C_5H_8 intermediate was taken as the sum of the collision energy and the chemical activation energy, where the latter is defined as the negative of the relative energy of the species with respect to the specific separated reactants. Rate constant calculations were performed at the zero-pressure limit using our in-house Unimol code[92] to replicate the single-collision conditions of the crossed molecular beam experiments. Finally, the branching ratios of the products were determined under the steady-state approximation using the RRKM-derived rate constants.[92,93]

3. RESULTS AND DISCUSSION

3.1. Laboratory Frame

Reactive scattering signal for the reaction of atomic carbon (C; 12 amu) with the butene isomers (C_4H_8; 56 amu) was monitored at the mass-to-charge (m/z) ratios of m/z = 67

https://doi.org/10.1021/acs.jpca.6c02765
J. Phys. Chem. A 2026, 130, 4823−4838

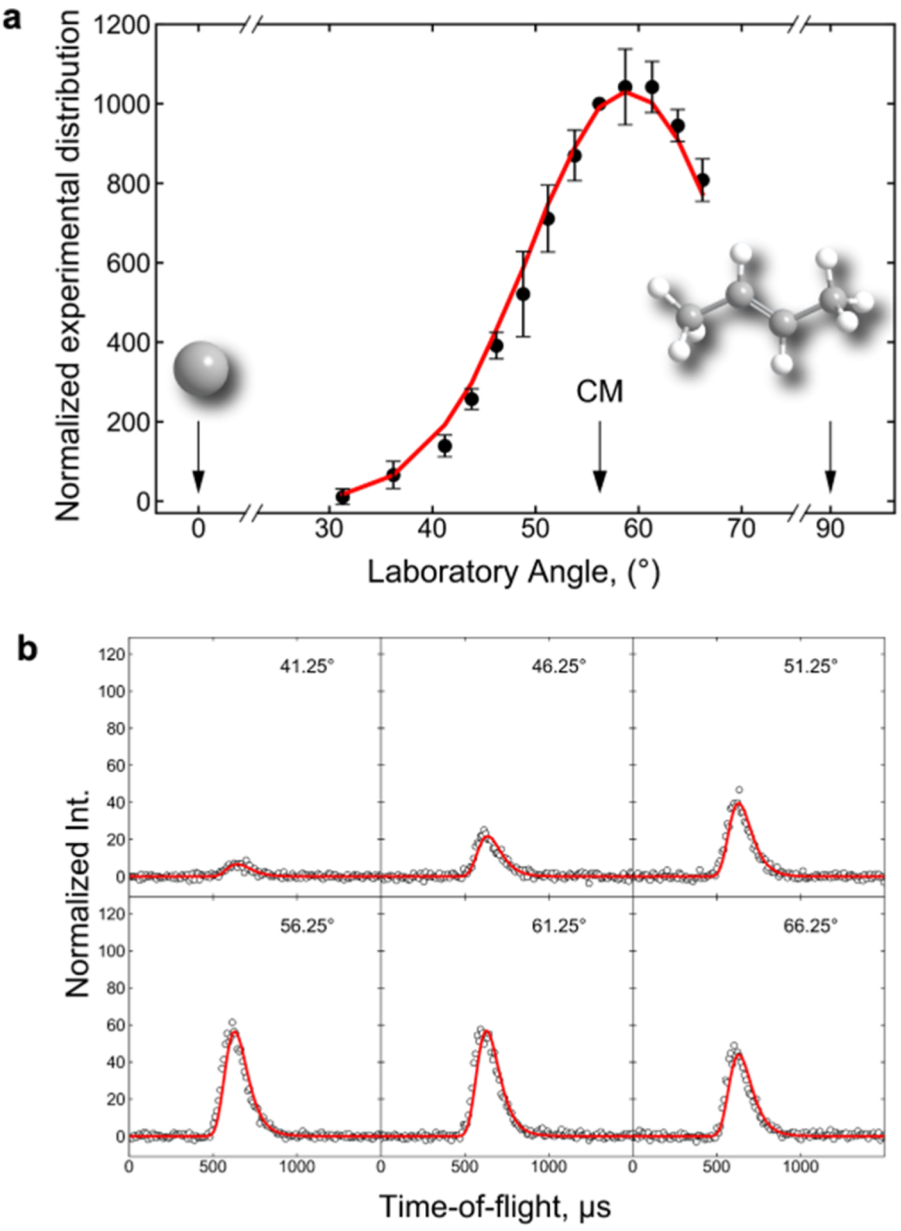

Figure 2. (a) Laboratory angular distribution and (b) time-of-flight (TOF) spectra recorded at $m/z = 66$ for the reaction of atomic carbon (C; ^3P_j) with *trans*-2-butene (C_4H_8; X^1A_g) at a collision energy of 28 ± 2 kJ mol^{-1}. The circles represent the experimental data, and the solid lines indicate the best fits obtained using the forward-convolution routine.

($C_5H_7^+$) and $m/z = 66$ ($C_5H_6^+$) for the atomic (reaction (1)) and molecular hydrogen (reaction (2)) loss pathways. High noise levels arising from fragmentation of the parent C_4H_8 ion prevented reliable detection of the methyl (CH_3) loss channel at $m/z = 53$.

$$C(12amu) + C_4H_8(56amu) \rightarrow C_5H_7(67amu) + H(1amu) \quad (1)$$

$$C(12amu) + C_4H_8(56amu) \rightarrow C_5H_6(66amu) + H_2(2amu) \quad (2)$$

Reactive scattering signal was successfully detected at both mass-to-charge ratios for all four butene isomers (1-butene, *cis*-2-butene, *trans*-2-butene, isobutene). However, the time-of-flight (TOF) profiles recorded at $m/z = 66$ and $m/z = 67$ were found to overlap after scaling (Figure S1), which suggests that the signal at $m/z = 66$ originates from the dissociative electron impact ionization of the parent C_5H_7 product ($m/z = 67$). Consequently, the TOF spectra for the reaction were collected at $m/z = 66$, which offered a better signal-to-noise ratio, at discrete intervals in steps of 2.5° from 26.25° to 66.25° Θ and integrated and normalized to obtain the laboratory angular distributions (LADs) (Figures 1−4). Integrated data accumulation times range up to 100 min per angle. All LADs for the C_4H_8 systems are symmetric around the center-of-mass (CM) angle, indicating that in the cases of all C_4H_8 isomers, the C_5H_7 products are formed via indirect scattering dynamics through the formation of one or more long-lived C_5H_8 intermediates.[69,94,95]

It is important to note the limitations of the used "universal" detector operated at 80 eV. While this setup provides for the broad monitoring of reactively scattered species, the high

https://doi.org/10.1021/acs.jpca.6c02765
J. Phys. Chem. A 2026, 130, 4823−4838

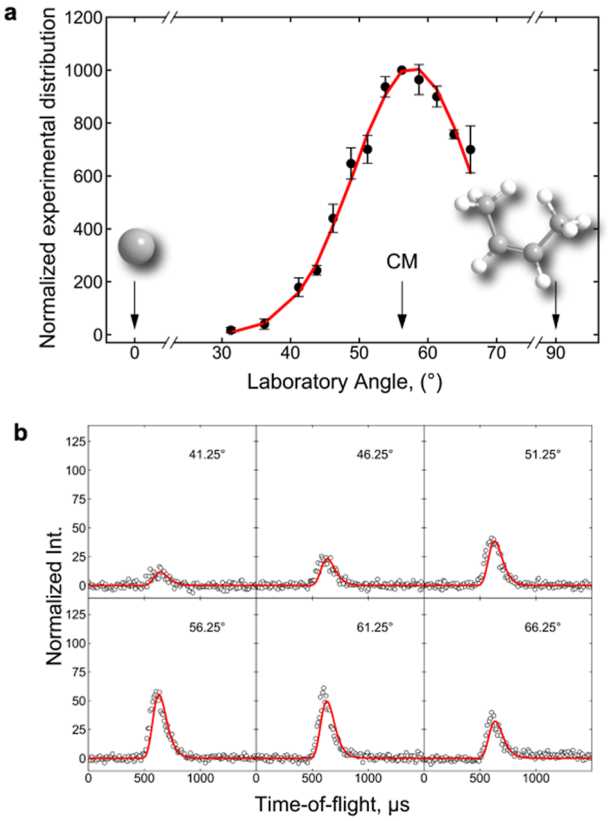

Figure 3. (a) Laboratory angular distribution and (b) time-of-flight (TOF) spectra recorded at m/z = 66 for the reaction of atomic carbon (C; ^3P_j) with *cis*-2-butene (C_4H_8; X^1A_1) at a collision energy of 28 ± 2 kJ mol^{-1}. The circles represent the experimental data, and the solid lines indicate the best fits obtained using the forward-convolution routine.

ionization energy leads to fragmentation of both the C_4H_8 reactant molecules and the reaction products. In our study, this fragmentation created a substantial background signal at m/z = 53 ($C_4H_5^+$) that effectively prevented detection of the methyl elimination channel due to the noise levels originating from the parent C_4H_8 isomers. Furthermore, the electron ionization lacks the capability for direct isomer discrimination. Consequently, the identification of the specific C_5H_7 product isomers relied on comparing the experimentally derived reaction energies with those obtained from high-level quantum chemical calculations (Sections 3.2 and 3.3).

3.2. Center-Of-Mass Frame

To further elucidate the reaction dynamics, the laboratory data were transformed into the center-of-mass (CM) reference frame using a forward-convolution routine.[77,78,96] The best-fit CM functions for all the systems are presented in Figures 5–8. The translational energy flux distribution P(E_T) (Figures 5a–8a) provides critical information regarding the reaction thermodynamics. For the reaction with 1-butene (Figure 5a), the derived P(E_T) distribution exhibits a maximum translational energy release (E_{max}) of 313 ± 16 kJ mol^{-1}. Energy conservation dictates that E_{max} is the sum of the collision energy (E_C) and the reaction exoergicity for those molecules born without internal excitation. Accounting for the average collision energy of 28 ± 2 kJ mol^{-1}, the reaction was determined to be exoergic by 285 ± 18 kJ mol^{-1}. Similar analyses for the remaining isomers yielded reaction energies of 203 ± 20 kJ mol^{-1} (*cis*-2-butene), 199 ± 20 kJ mol^{-1} (*trans*-2-butene), and 230 ± 18 kJ mol^{-1} (isobutene). On average, between all systems, approximately 24% of the total available energy is channeled into the translational degrees of freedom of the products, which is consistent with the formation of a covalently bound C_5H_8 intermediate (indirect scattering dynamics).

The center-of-mass angular distribution T(θ) (Figures 5b–8b) offers additional insights into the scattering process. These systems reveal forward–backward symmetry with respect to 90°, a feature characteristic of an indirect reaction mechanism involving long-lived C_5H_8 intermediates that have a lifetime longer than their rotational period.[79] These dynamics are also captured in the flux contour map (Figures 5c–8c), which provides a comprehensive image of the reactive scattering probability across all angles and kinetic energies.

3.3. Potential Energy Surface

We merge now the experimental data with electronic structure and statistical calculations to provide insights into the chemical dynamics and reaction mechanisms of ground-state atomic carbon (C, ^3P_j) reacting with four C_4H_8 isomers: *cis*-2-butene (X^1A_1), *trans*-2-butene (X^1A_g), isobutene (X^1A_1), and 1-butene (X^1A). Computations discovered 45 reaction intermediates leading to 29 feasible, distinct products on the triplet potential energy surface (PES) (Figures 9–11, S2–S7).

The experimentally derived reaction energies ($\Delta_r G$) for the atomic hydrogen loss pathway are −285 ± 18 kJ mol^{-1} (1-butene), −203 ± 21 kJ mol^{-1} (*cis*-2-butene), −199 ± 21 kJ mol^{-1} (*trans*-2-butene), and −230 ± 19 kJ mol^{-1} (isobutene). These values exhibit excellent agreement with the calculated reaction energies for the formation of distinct resonantly stabilized C_5H_7 radicals on their respective PESs (Figures 9–11). Specifically, for the 1-butene system, the derived energy strongly supports the formation of the **p3** isomer (1-vinylallyl), which is calculated to be exoergic by 286 kJ mol^{-1}. In the case of isobutene, the experimental reaction energy aligns with the formation of the **p7** (2-vinylallyl) isomer located at −234 kJ mol^{-1}. For the *cis*- and *trans*-2-butene systems, the derived energies are consistent with the prevalence of the **p2** isomer (1,3-dimethylpropargyl), which has a theoretical exoergicity of 201 kJ mol^{-1}. While multiple hydrogen atom loss channels are thermodynamically accessible across all four isomers, alternative products with lower associated exoergicities (**p4** for 2-butenes, **p6**/**p8** for isobutene, or **p11** for 1-butene) forming with potentially significant branching ratios may be masked in the lower-energy portion of the translational energy flux distributions P(E_T).

3.3.1. *Cis*- and *trans*-2-Butene. Let us first consider the reactions of atomic carbon with the *cis*- and *trans*-2-butene isomers (Figure 9). The reactions are initiated by a barrierless addition of atomic carbon to the π-electron density of the C=C bond of the C_4H_8 molecules, yielding triplet carbene intermediates **i1** and **i2** incorporating three-membered rings. These intermediates are stabilized by 226 and 222 kJ mol^{-1}, respectively, relative to C + *trans*-2-butene. Notably, *cis*-2-butene is only 5 kJ mol^{-1} higher in energy than its *trans* counterpart. Subsequently, the cleavage of the former CH=CH double bonds via ring-opening occurs via moderate barriers of 53 and 58 kJ mol^{-1} and leads to triplet acyclic intermediates **i3** (*syn*–*anti*) and **i5** (*anti*–*anti*), which can be described as triplet 1,3-dimethylallenes. The two unpaired electrons in the triplet state, predominantly localized on the

https://doi.org/10.1021/acs.jpca.6c02765
J. Phys. Chem. A 2026, 130, 4823–4838

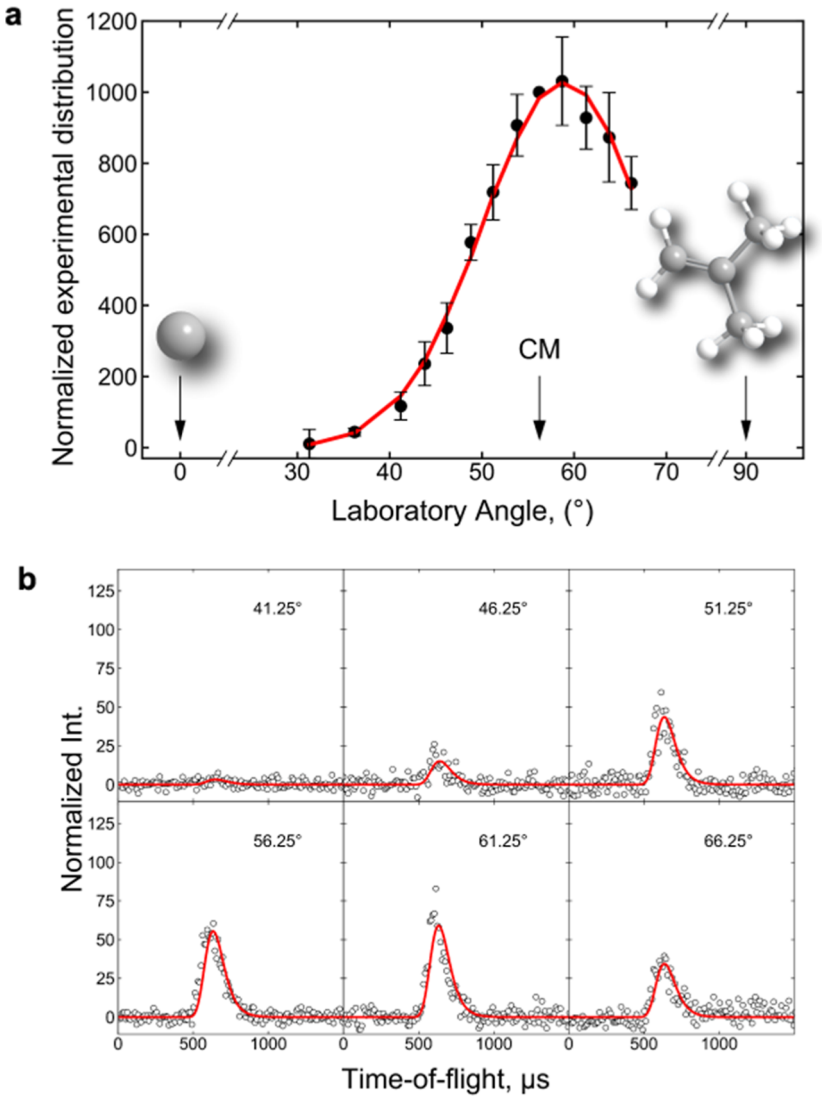

Figure 4. (a) Laboratory angular distribution and (b) time-of-flight (TOF) spectra recorded at $m/z = 66$ for the reaction of atomic carbon (C; ^3P_j) with isobutene (C_4H_8; X^1A_1) at a collision energy of 28 ± 2 kJ mol^{-1}. The circles represent the experimental data, and the solid lines indicate the best fits obtained using the forward-convolution routine.

two terminal carbon atoms of the allene moiety, experience significant mutual repulsion. To minimize this repulsion, the triplet allene framework adopts a bent, planar geometry in contrast to the linear twisted structure of the singlet ground state.

Thus, the overall transformation—barrierless carbon-atom addition to the C═C bond followed by cleavage of the original double bond and ring opening—embodies a *de facto* insertion mechanism of atomic carbon into the carbon−carbon double bond of unsaturated hydrocarbons. Relative to the separated reactants, the transition states leading to **i3** and **i5** lie rather deep on the PES. Moreover, from **i1** and **i2**, no alternative pathways other than the three-membered ring opening are thermodynamically feasible; hydrogen migrations from the CH_3 groups to the bare carbon atom could not compete with the aforementioned channel. Insertions of atomic carbon into carbon−hydrogen bonds were found not to be competitive either.

Further, **i3** and **i5** can undergo isomerization to the *syn*−*syn* isomer **i4** via a barrier of some 100 kJ mol^{-1}. **i4** is less stable due to the steric repulsion between the two CH_3 groups, which, among the three conformers, are positioned closest to each other in **i4**. For **i3**, both hydrogen atom and methyl loss channels are accessible, leading to 1,3-dimethylpropargyl (**p2**) and 1-methylpropargyl (**p1**), respectively. Thermodynamically, the methyl elimination channel via the β-scission mechanism is favored, as **p1** lies 33 kJ mol^{-1} below **p2**, and the transition state for methyl loss is slightly lower in energy than that for hydrogen atom elimination. Both **p1** and **p2** are formed via tight exit transition states, which reside 43 and 19 kJ mol^{-1} above the respective separated products **p1** + CH_3 and **p2** + H. In contrast, **i4** decomposes exclusively to **p1** + CH_3, whereas **i5** yields **p2** + H through tight exit transition states analogous to those found for **i3**. In all three conformers **i3**−**i5**, an H atom elimination from a methyl group leads to product **p4** (1-methyl-buta-1,3-dien-2-yl) via the highest energy barriers, proceeding through tight exit transition states that lie 40, 50, and 36 kJ mol^{-1} above the separated products **p4** + H.

An alternative pathway involves a [1,3]-hydrogen migration from either of the two methyl groups in **i5**, but from only one methyl group in **i3**, to the bare central carbon atom, forming the triplet *trans*-1,3-pentadiene (**i6**). Energetically, this process

https://doi.org/10.1021/acs.jpca.6c02765
J. Phys. Chem. A 2026, 130, 4823−4838

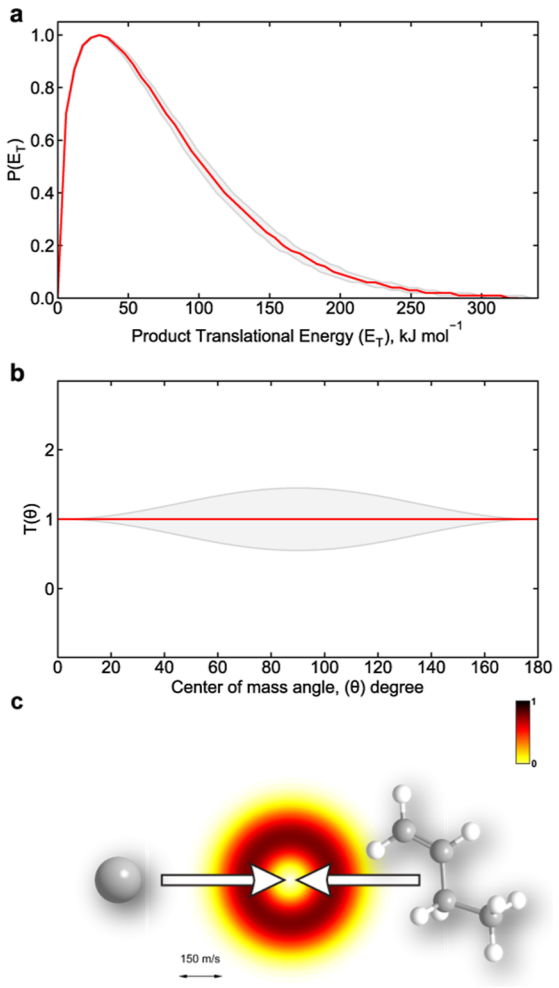

Figure 5. (a) Center-of-mass translational energy $P(E_T)$, (b) angular $T(\theta)$ flux distributions, and (c) flux contour map for the reaction of atomic carbon (C; ^3P_j) with 1-butene (C_4H_8; X^1A) at a collision energy of 28 ± 2 kJ mol^{-1}. The solid lines represent the best fits obtained via the forward-convolution routine, while the shaded areas indicate the range of acceptable fits. For the angular distribution (b), the direction of the atomic carbon beam is defined as 0° and the 1-butene beam as 180°.

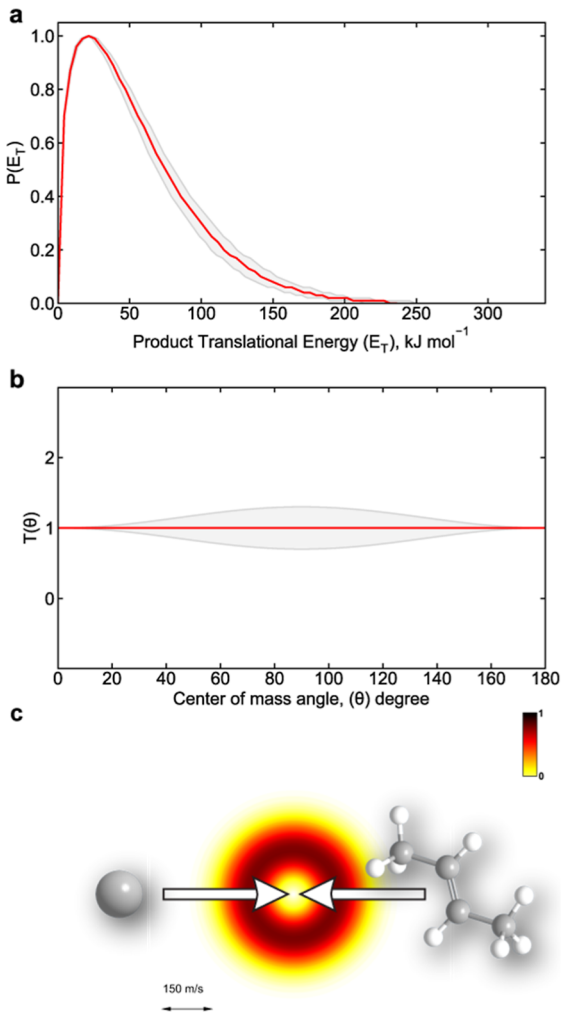

Figure 6. (a) Center-of-mass translational energy $P(E_T)$, (b) angular $T(\theta)$ flux distributions, and (c) flux contour map for the reaction of atomic carbon (C; ^3P_j) with *trans*-2-butene (C_4H_8; X^1A_g) at a collision energy of 28 ± 2 kJ mol^{-1}. The solid lines represent the best fits obtained via the forward-convolution routine, while the shaded areas indicate the range of acceptable fits. For the angular distribution (b), the direction of the atomic carbon beam is defined as 0° and the *trans*-2-butene beam as 180°.

is competitive with the hydrogen atom and methyl loss channels. Rotation around the partial C═C double bond in **i6** proceeds via a barrier of 60 kJ mol^{-1} and affords the *cis* isomer **i7**. H atom elimination from the remaining methyl group in either **i6** or **i7** can generate product **p3** (1-vinylallyl), which is 40 kJ mol^{-1} more stable than **p1**.

Finally, although a [1,2]-H shift from the CH group to the adjacent CH_2 moiety interconnecting **i6** and **i7** with **i8** are energetically comparable to the hydrogen atom and methyl loss channels affording **p1** and **p2**, a [1,4]-H shift from the CH group, adjacent to the CH_3 moiety, to the CH_2 group connecting **i7** to **i9** via a barrier of 100 kJ mol^{-1}—comparable to the rotational barriers around the partial double bonds in **i3**−**i5**, is more favorable. Both intermediates **i8** and **i9**, which are interconnected by a rotational barrier of 60 kJ mol^{-1}, dissociate to **p2** + H through tight exit transition states lying 16 and 14 kJ mol^{-1}, respectively, above the separated products.

3.3.2. Isobutene. The reaction of the atomic carbon with isobutene (Figure 10) proceeds through a mechanism that closely resembles the two systems described above for the *cis*/*trans*-2-butenes. Barrierless addition of C to the C═C double bond of isobutene yields intermediate **i10**, with an energy of −224 kJ mol^{-1} relative to the reactants, similar to that of **i1** and **i2**. Subsequently, **i10** undergoes ring opening via a barrier of 58 kJ mol^{-1} to afford the triplet 1,1-dimethylallene **i11** intermediate. It should be noted that any direct hydrogen migration from a methyl group to the bare carbon atom of the three-membered ring in **i10**, bypassing the ring opening to **i11**, proceeds through prohibitively high barriers, making this pathway kinetically negligible under crossed molecular beam conditions.

A loss of either methyl group from **i11** leads to product **p5** (3-methylpropargyl) through a tight exit transition state located 48 kJ mol^{-1} above the energy of the separated products **p5** + H. In the two previous reactions, analogous methyl elimination afforded 1-methylpropargyl with a reverse barrier of 43 kJ mol^{-1}. By contrast, hydrogen atom loss from the CH_2 group in **i11** generates **p6** (1,1-dimethylpropargyl) via a tight exit transition state situated 16 kJ mol^{-1} above the

https://doi.org/10.1021/acs.jpca.6c02765
J. Phys. Chem. A 2026, 130, 4823−4838

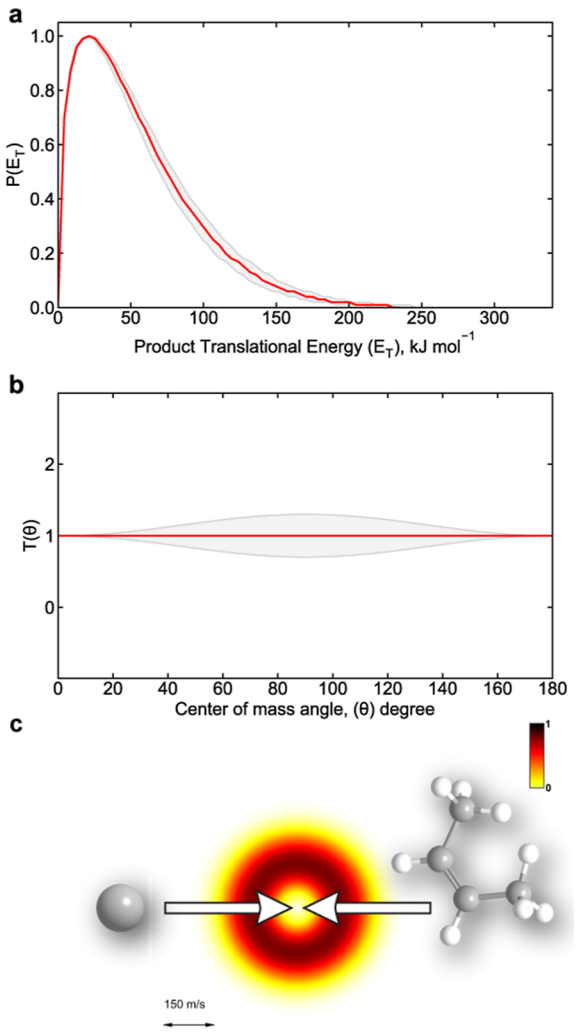

Figure 7. (a) Center-of-mass translational energy $P(E_T)$, (b) angular $T(\theta)$ flux distributions, and (c) flux contour map for the reaction of atomic carbon (C; ^3P_j) with *cis*-2-butene (C_4H_8; X^1A_1) at a collision energy of 28 ± 2 kJ mol^{-1}. The solid lines represent the best fits obtained via the forward-convolution routine, while the shaded areas indicate the range of acceptable fits. For the angular distribution (b), the direction of the atomic carbon beam is defined as 0° and the *cis*-2-butene beam as 180°.

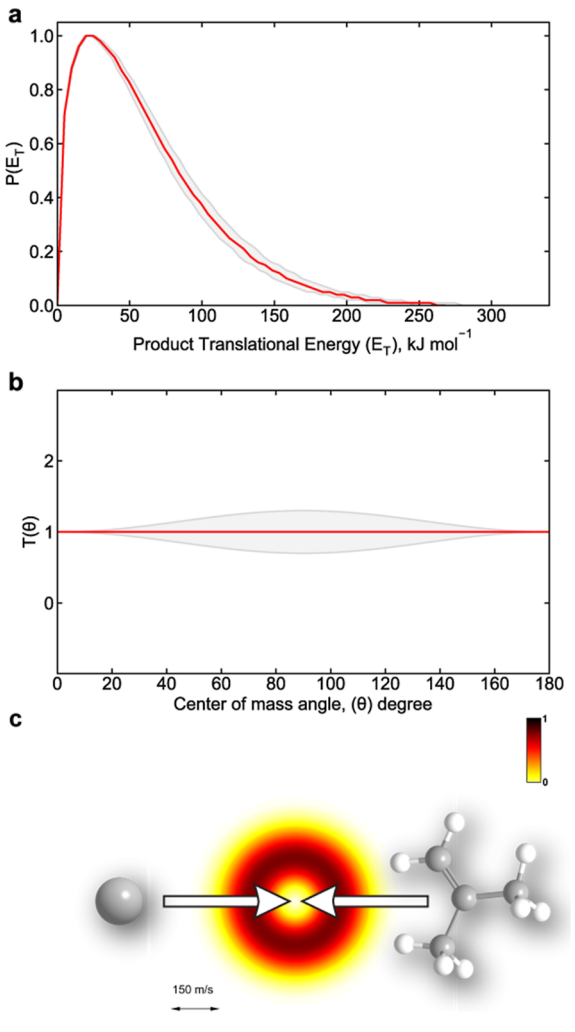

Figure 8. (a) Center-of-mass translational energy $P(E_T)$, (b) angular $T(\theta)$ flux distributions, and (c) flux contour map for the reaction of atomic carbon (C; ^3P_j) with isobutene (C_4H_8; X^1A_1) at a collision energy of 28 ± 2 kJ mol^{-1}. The solid lines represent the best fits obtained via the forward-convolution routine, while the shaded areas indicate the range of acceptable fits. For the angular distribution (b), the direction of the atomic carbon beam is defined as 0° and the isobutene beam as 180°.

separated products **p6** + H. For the 2-butene reactions, the corresponding product was 1,3-dimethylpropargyl with a reverse barrier of 19 kJ mol^{-1}.

3.3.3. 1-Butene. The PES for the reaction of atomic carbon with 1-butene is illustrated in Figure 11. Initially, barrierless addition of atomic carbon to the C=C double bond of 1-butene generates adduct **i16** (−226 kJ mol^{-1}), whose energy is very similar to that of the adducts formed in the reactions of the other butene isomers. Overcoming a barrier of 60 kJ mol^{-1} affords the triplet 1-ethylallene in its *gauche* form, **i17**. Passing through a barrier of approximately 100 kJ mol^{-1} then converts **i17** into the *cis* isomer **i18**. It should be noted that, although **i16** offers a comparatively favorable pathway—a shift from the CH_3 group to the bare carbon of the three-membered ring (Figure S7), with a barrier only 30 kJ mol^{-1} higher than that for ring opening to **i17**—this route does not ultimately compete with the **i16**−**i17** channel. Nevertheless, the reaction of 1-butene with atomic carbon is distinguished by an abundance of favorable channels and, consequently, a diverse product distribution. Moreover, one of the most thermodynamically favorable pathways is exclusive to this system.

Returning to intermediates **i17** and **i18**, an entropically more favorable pathway for these species is β-scission of the C−C bond via methyl loss, leading to product **p10** (buta-1,3-dien-2-yl) through tight exit transition states located 65 and 57 kJ mol^{-1} above the separated products **p10** + CH_3. Another option for **i17** is ethyl elimination, also proceeding via β-scission, which affords propargyl (**p9**) through a tight exit transition state lying 39 kJ mol^{-1} above the separated products **p9** + C_2H_5. A hydrogen atom loss from any of the CH_2 groups in **i19** and **i20** connects them to product **p11** (1-ethylpropargyl) via tight exit transition states lying 17 kJ mol^{-1} above **p11** + H, and to **p13** ((Z)-4-methyl-buta-1,3-dien-2-yl) via tight exit transition states residing 51 and 43 kJ mol^{-1} above **p13** + H. In contrast, hydrogen atom loss from the CH group in **i18** leads to **p14** (3-ethylpropargyl) through a tight exit transition state located 17 kJ mol^{-1} above **p14** + H.

https://doi.org/10.1021/acs.jpca.6c02765
J. Phys. Chem. A 2026, 130, 4823−4838

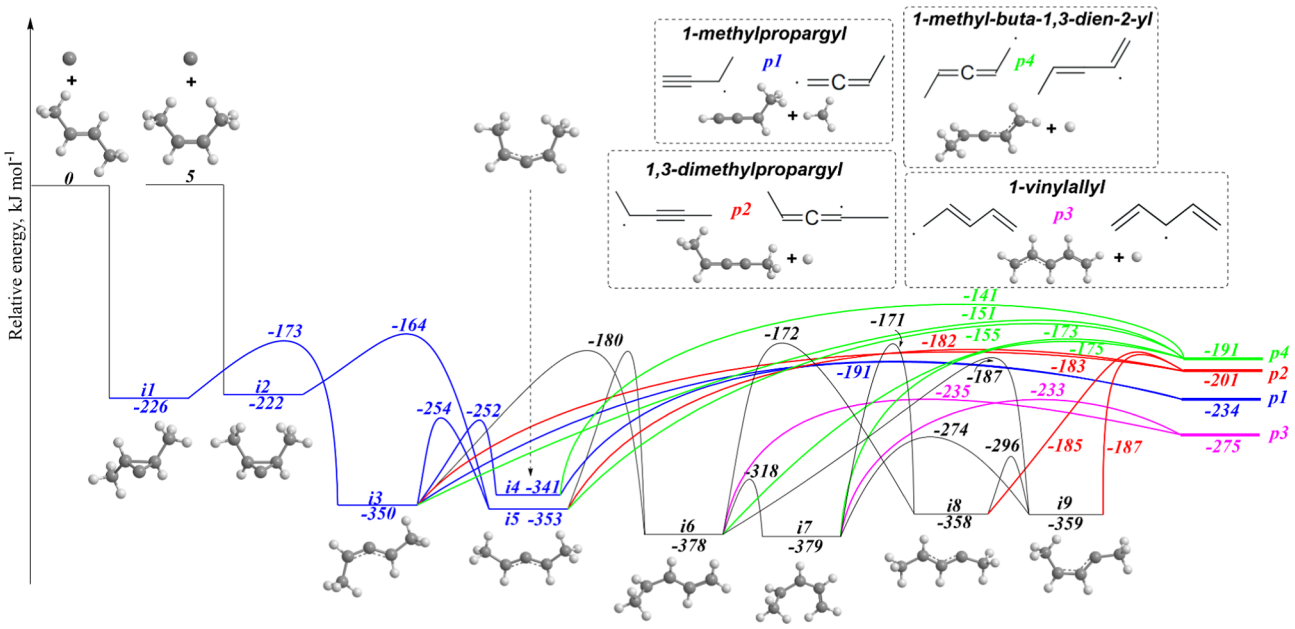

Figure 9. Potential energy surface for the bimolecular reaction of the ground-state atomic carbon (C, ^3P_j) with *cis*-2-butene (C_4H_8, X^1A_1) and *trans*-2-butene (C_4H_8, X^1A_g) calculated at the CCSD(T)-F12/cc-pVTZ-f12//ωB97X-D/6-311G(d,p) + ZPE(ωB97X-D/6-311G(d,p)) level of theory. The dominating channel predicted by RRKM calculations is colored in blue.

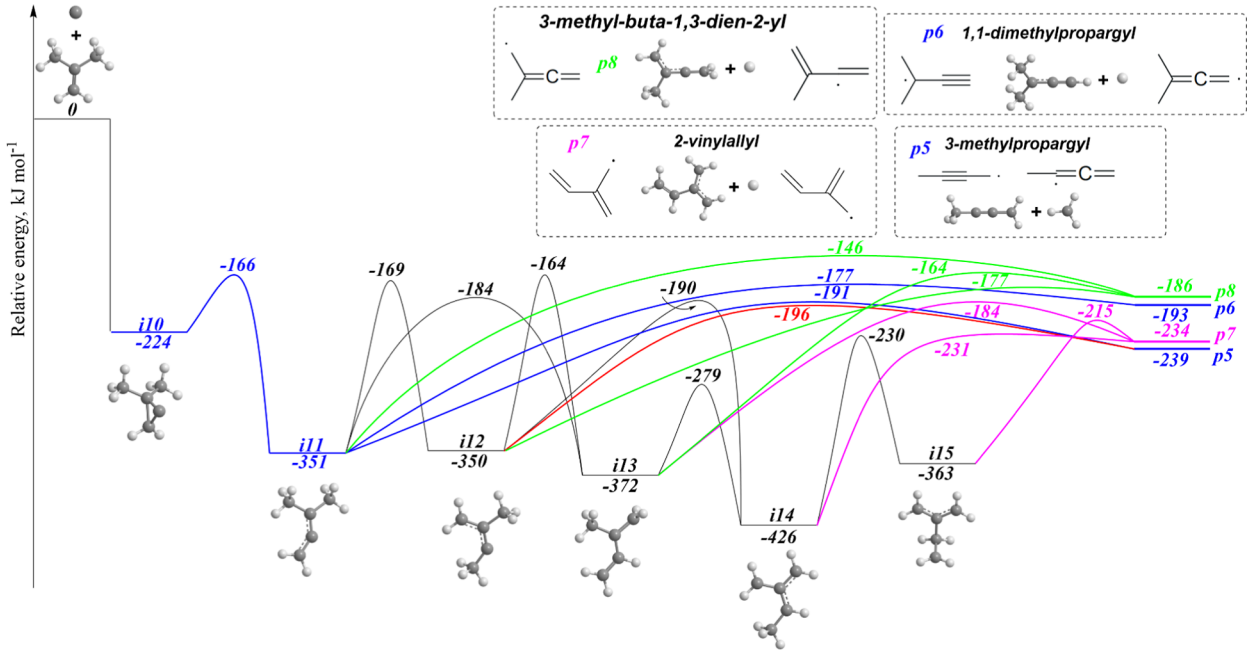

Figure 10. Potential energy surface for the bimolecular reaction of the ground-state atomic carbon (C, ^3P_j) with isobutene (C_4H_8, X^1A_1) calculated at the CCSD(T)-F12/cc-pVTZ-f12//ωB97X-D/6-311G(d,p) + ZPE(ωB97X-D/6-311G(d,p)) level of theory. The dominating channel predicted by RRKM calculations is colored in blue.

The lowest transition state (−199 kJ mol^{-1} for **i17** → **p9**) for entropically favorable fragmentation channels in **i17** is at least 73 kJ mol^{-1} higher than the unique, enthalpically most favorable pathway identified for this reaction, the **i18** → **i19** transformation via a [1,4]-H migration from the terminal CH_3 group to the bare carbon atom. This pathway can also readily compete with the entropically favorable fragmentations in **i18**, where the lowest-lying transition state (−190 kJ mol^{-1} for **i18** → **p10**) is 82 kJ mol^{-1} above the barrier for the **i18** → **i19** transformation. The latter channel opens a pathway to product **p3** (1-vinylallyl), which was negligible in the reactions with 2-butenes. **i19** can readily convert to **i20** via a moderate rotational barrier of 63 kJ mol^{-1}. Both **i19** and **i20** decompose to **p3** + H through tight exit transition states located 16 and 22 kJ mol^{-1} above the separated products. Moreover, these transition states lie at least 17 kJ mol^{-1} below the energies of all products considered in Figure 11. An alternative, less likely scenario for **i19** and **i20** is triplet methylene elimination, leading to **p12** (1,3-butadiene) via tight transition states lying 12 and 22 kJ mol^{-1} above the separated products **p12** + CH_2.

https://doi.org/10.1021/acs.jpca.6c02765
J. Phys. Chem. A 2026, 130, 4823−4838

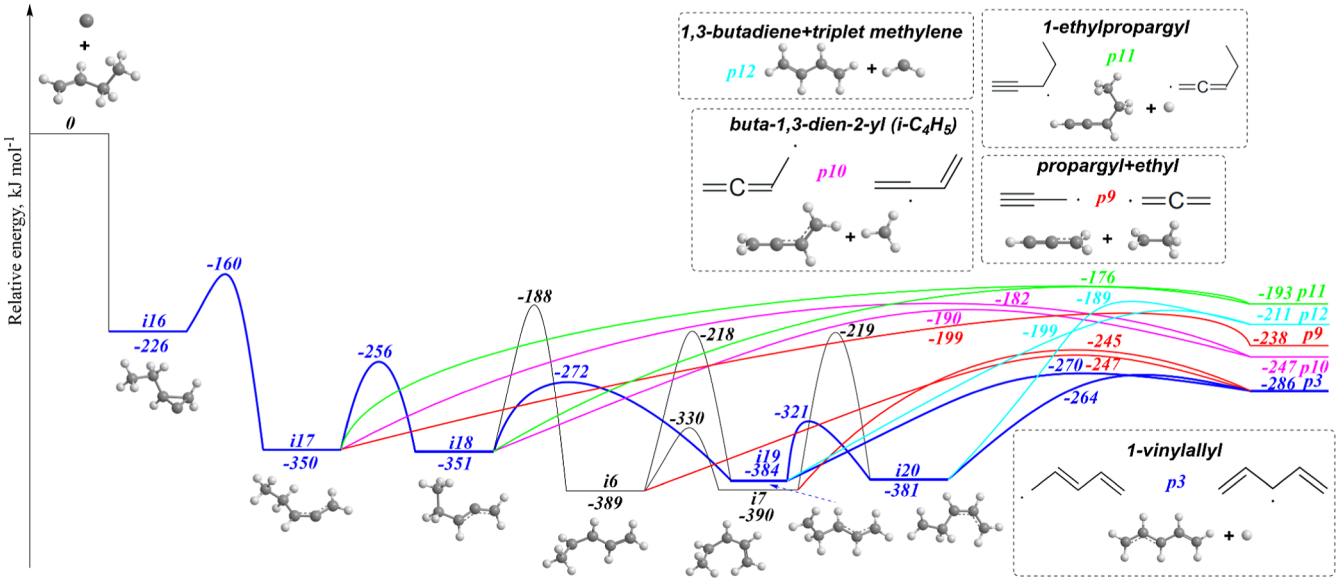

Figure 11. Potential energy surface for the bimolecular reaction of the ground-state atomic carbon (C, ^3P_j) with 1-butene (C_4H_8, X^1A) calculated at the CCSD(T)-F12/cc-pVTZ-f12//ωB97X-D/6−311G(d,p) + ZPE(ωB97X-D/6-311G(d,p)) level of theory. The dominating channel predicted by RRKM calculations is colored in blue.

Table 1. Product Branching Ratios (%) from RRKM Calculations for the Reactions of Atomic Carbon (C, ^3P_j) with *trans*-2-Butene (X^1A_g), *cis*-2-Butene (X^1A_1), Isobutene (X^1A_1), and 1-Butene (X^1A) at the Zero-Collision-Energy Limit and at the Experimental Collision Energy (E_C, kJ mol^{-1})

reactants		C + *trans*-2-butene		C + *cis*-2-butene		C + isobutene		C + 1-butene	
E_C		0	28	0	28	0	28	0	28
product notation	product name	ratios							
p1	1-methylpropargyl + CH_3	89.7	88.8	81.4	76.1	0.0	0.0	0.0	0.0
p2	1,3-dimethylpropargyl + H	8.9	9.5	15.9	20.2	0.0	0.0	0.2	0.3
p3	1-vinylallyl + H	0.7	0.7	1.2	1.4	0.0	0.0	50.1	37.5
p4	1-methyl-buta-1,3-dien-2-yl + H	0.7	0.9	1.4	2.2	0.0	0.0	0.0	0.0
p5	3-methylpropargyl + CH_3	0.0	0.0	0.0	0.0	53.2	50.2	0.0	0.0
p6	1,1-dimethylpropargyl + H	0.0	0.0	0.0	0.0	40.5	43.8	0.0	0.0
p7	2-vinylallyl + H	0.0	0.0	0.0	0.0	5.5	5.0	0.0	0.0
p8	3-methyl-buta-1,3-dien-2-yl + H	0.0	0.0	0.0	0.0	0.4	0.6	0.0	0.0
p9	propargyl + C_2H_5	0.0	0.0	0.0	0.0	0.0	0.0	22.5	26.5
p10	buta-1,3-dien-2-yl + CH_3	0.0	0.0	0.0	0.0	0.2	0.2	11.3	14.9
p11	1-ethylpropargyl + H	0.0	0.0	0.0	0.0	0.0	0.0	8.5	12.2
p12	1,3-butadiene + triplet CH_2	0.0	0.0	0.0	0.0	0.0	0.0	5.5	6.0
p13	(Z)-4-methyl-buta-1,3-dien-2-yl + H	0.0	0.1	0.1	0.1	0.0	0.0	0.6	1.0
p14	3-ethylpropargyl + H	0.0	0.0	0.0	0.0	0.0	0.0	0.9	1.2
p16	cyclopenten-3-yl + H	0.0	0.0	0.0	0.0	0.0	0.0	0.3	0.2
p25	ethylene + triplet allene	0.0	0.0	0.0	0.0	0.2	0.2	0.0	0.0
p29	triplet ethylene + methylacetylene	0.0	0.0	0.0	0.0	0.0	0.0	0.1	0.2

3.3.4. RRKM Calculations. What are the major reaction products? RRKM calculations were carried out at two collision energies: the zero-collision-energy limit, mimicking low-temperature conditions in cold molecular clouds, and the experimental value of 28 kJ mol^{-1} (the product branching ratios are shown in Table 1, and the rate constants are given in Tables S1−S4). For the reactions of atomic carbon with the *cis*- and *trans*-2-butene isomers, the calculations predict that the entropically favored β-scission channel—involving CH_3 loss from intermediates **i3** and **i4**—dominates (pathways 3 and 4), affording RSFR product **p1** (1-methylpropargyl) with branching ratios of approximately 80% and 90%, respectively. As expected, the hydrogen atom elimination channel from a CH group in intermediates **i3** and **i5** follows (pathways 5 and 6), yielding an RSFR product **p2** (1,3-dimethylpropargyl) with branching fractions of about 20% and 10%, respectively. These results indicate that further hydrogen migrations cannot compete with these rapid fragmentation pathways from the triplet 1,3-dimethylallene conformers **i3**−**i5**. Otherwise, the formation of intermediate **i6** would have enhanced the yield of the thermodynamically most stable RSFR product **p3** (1-vinylallyl) (Figure 9), which in our case amounts to only 1% (pathways 7 and 8).

$$C(^3P_j) + \text{trans-2-butene} \rightarrow \mathbf{i1} \rightarrow [\mathbf{i3}]/[\mathbf{i3} \rightarrow \mathbf{i4}] \rightarrow \mathbf{p1} + CH_3 \quad (3)$$

https://doi.org/10.1021/acs.jpca.6c02765
J. Phys. Chem. A 2026, 130, 4823−4838

$$C(^3P_j) + \text{cis-2-butene} \rightarrow \mathbf{i2} \rightarrow \mathbf{i5} \rightarrow [\mathbf{i3}]/[\mathbf{i3} \rightarrow \mathbf{i4}] \rightarrow \mathbf{p1} + CH_3 \quad (4)$$

$$C(^3P_j) + \text{trans-2-butene} \rightarrow \mathbf{i1} \rightarrow [\mathbf{i3}]/[\mathbf{i3} \rightarrow \mathbf{i5}] \rightarrow \mathbf{p2} + H \quad (5)$$

$$C(^3P_j) + \text{cis-2-butene} \rightarrow \mathbf{i2} \rightarrow [\mathbf{i5}]/[\mathbf{i5} \rightarrow \mathbf{i3}] \rightarrow \mathbf{p2} + H \quad (6)$$

$$C(^3P_j) + \text{trans-2-butene} \rightarrow \mathbf{i1} \rightarrow [\mathbf{i3}]/[\mathbf{i3} \rightarrow \mathbf{i5}] \rightarrow \mathbf{i6} \rightarrow \mathbf{p3} + H \quad (7)$$

$$C(^3P_j) + \text{cis-2-butene} \rightarrow \mathbf{i2} \rightarrow [\mathbf{i5}]/[\mathbf{i5} \rightarrow \mathbf{i3}] \rightarrow \mathbf{i6} \rightarrow \mathbf{p3} + H \quad (8)$$

Turning to the atomic carbon plus isobutene reaction, the same trend as in the two previously discussed reactions is observed, yet with a notable difference: the branching ratios for CH_3 and H elimination are close to one another (Table 1). The entropically advantageous β-scission channel—methyl loss from the 1,1-dimethylallene species **i11**—barely outcompetes its counterpart, delivering the thermodynamically most stable product RSFR **p5** (3-methylpropargyl) (Figure 10, pathway 9) with a branching ratio marginally over 50%. Meanwhile, an H atom loss from CH_2 in the same intermediate **i11**, which produces RSFR **p6** (1,1-dimethylpropargyl), contributes slightly more than 40% (pathway 10). These results further underscore the insignificance of hydrogen shift reaction steps; if such rearrangements were competitive, RSFR product **p7** (2-vinylallyl), which is energetically more favorable than **p6** and arises from an H atom elimination from CH_3 in **i13**, would be formed in a larger proportion (pathway 11).

$$C(^3P_j) + \text{isobutene} \rightarrow \mathbf{i10} \rightarrow \mathbf{i11} \rightarrow \mathbf{p5} + CH_3 \quad (9)$$

$$C(^3P_j) + \text{isobutene} \rightarrow \mathbf{i10} \rightarrow \mathbf{i11} \rightarrow \mathbf{p6} + H \quad (10)$$

$$C(^3P_j) + \text{isobutene} \rightarrow \mathbf{i10} \rightarrow \mathbf{i11} \rightarrow [\mathbf{i13}]/[\mathbf{i13} \rightarrow \mathbf{i14}] \rightarrow \mathbf{p7} + H \quad (11)$$

For the atomic carbon plus 1-butene reaction, statistical calculations reveal a unique picture among all C_4H_8 isomers studied, an "overt competition" between entropic (ΔS) and enthalpic (ΔH) factors governing the reaction outcome. The H atom loss channel prevails (Table 1), leading to the thermodynamically most favorable product, **p3** (1-vinylallyl), with a relative yield of 37.5% at the experimental collision energy of 28 kJ mol^{-1}, which rises to 50% in the zero-collision-energy limit (pathway 12). This pathway is highlighted in blue in Figure 11. A distinctive feature of this reaction is an additional hydrogen migration (**i18** → **i19**), which counteracts the entropic contribution from rapid H, CH_3, or C_2H_5 losses from the triplet 1-ethylallene intermediates **i17** and **i18** (pathways 13−15). The second significant channel (pathway 14) is C_2H_5 elimination from **i17**, which accounts for up to about 26% at E_C = 28 kJ mol^{-1} and affords **p9** (propargyl). Next is CH_3 loss from **i17** or **i18**, leading to product **p10** (buta-1,3-dien-2-yl) with a yield of up to 15% at E_C = 28 kJ mol^{-1}. A non-negligible contribution of approximately 12% at the same collision energy comes from H atom loss in **i17** or **i18**, yielding **p11** (1-ethylpropargyl). Notably, the combined contribution of propargyl-family radicals (**p9**, **p11**, **p14** (3-ethylpropargyl)) amounts to about 40%, which slightly outweighs the yield of the allyl-type radical.

$$C(^3P_j) + \text{1-butene} \rightarrow \mathbf{i16} \rightarrow \mathbf{i17} \rightarrow \mathbf{i18} \rightarrow [\mathbf{i19}]/[\mathbf{i19} \rightarrow \mathbf{i20}] \rightarrow \mathbf{p3} + H \quad (12)$$

$$C(^3P_j) + \text{1-butene} \rightarrow \mathbf{i16} \rightarrow [\mathbf{i17}]/[\mathbf{i17} \rightarrow \mathbf{i18}] \rightarrow \mathbf{p10} + CH_3/\mathbf{p11} + H/\mathbf{p13} + H \quad (13)$$

$$C(^3P_j) + \text{1-butene} \rightarrow \mathbf{i16} \rightarrow \mathbf{i17} \rightarrow \mathbf{p9} + C_2H_5 \quad (14)$$

$$C(^3P_j) + \text{1-butene} \rightarrow \mathbf{i16} \rightarrow \mathbf{i17} \rightarrow \mathbf{i18} \rightarrow \mathbf{p14} + H \quad (15)$$

In summary, the presence of alkyl substituents in the alkene reactant significantly changes the product spectrum of atomic carbon reactions. For the simplest case, $C(^3P_j) + C_2H_4$, only hydrogen atom loss is accessible, exclusively affording the propargyl radical.[21] As the alkene size increases from C_2H_4[60−65] to C_3H_6[60,66,67] and further to the C_4H_8 isomers (*cis*-/*trans*-2-butene and isobutene), an additional fragmentation channel—methyl loss—emerges and becomes competitive, yielding propargyl along with methyl-substituted propargyl radicals. RRKM calculations confirm the significant contribution of this β-scission pathway. Notably, across the reactions with *cis*-2-butene, *trans*-2-butene, and isobutene, the methyl groups act solely as spectators; no hydrogen migrations from the methyl moieties contribute measurably to the product distribution. The only exception is the reaction with 1-butene, where a single hydrogen shift from the terminal CH_3 group redirects the entire reaction course. Furthermore, in the 1-butene system, methyl loss does not afford a propargyl-type radical; instead, only H atom and ethyl loss channels operate, leading to propargyl itself and to ethyl-substituted propargyl radicals.

It should be emphasized that statistical theories such as RRKM apply to rate constant calculations only when the system has sufficient time to undergo intramolecular vibrational relaxation (IVR); that is, IVR must proceed faster than the competing isomerization and/or dissociation processes. For medium-sized species such as C_5H_8 intermediates on the PESs (typically systems with ∼10−30 atoms), IVR is expected to occur on a picosecond time scale. Consequently, the RRKM theory remains valid as long as the reaction rate constants do not exceed the limit of $\sim 10^{13}$ s^{-1}. Here, we cannot explicitly claim that the reaction behaves statistically in reality; however, the reaction likely satisfies the RRKM conditions, given that we observe good agreement between the experimentally measured energy release and the theoretically computed one. Moreover, in the two reactions forming 1- and 2-vinylallyl isomers (**p3** and **p7**; Figures 10 and 11), where this agreement is observed, at least 2 to 4 isomerization steps must be overcome prior to the dissociation of the intermediates into these products.

4. CONCLUSIONS

In this study, we have investigated the reactions of ground-state atomic carbon (C, ^3P_j) with all four butene isomers (1-butene, *cis*-2-butene, *trans*-2-butene, and isobutene) under single-collision conditions using crossed molecular beams and high-level quantum chemical calculations. These exoergic

https://doi.org/10.1021/acs.jpca.6c02765
J. Phys. Chem. A 2026, 130, 4823−4838

reactions proceed via a barrierless addition of atomic carbon to the alkene C=C bond, triggering ring opening to substituted triplet allene intermediates followed by decomposition through H, CH_3, or C_2H_5 loss, yielding a family of propargyl-type resonance-stabilized free radicals (RSFRs). These reactions are thus accessible even in low-temperature environments, particularly in cold molecular clouds (10 K). Crossed molecular beam experiments were conducted at a mean collision energy of 28 ± 2 kJ mol^{-1}, and this energy was taken to evaluate energy-dependent rate constants within the Rice−Ramsperger−Kassel−Marcus (RRKM) approach to replicate the single-collision conditions of the experiments. It should be noted that for the C + C_4H_8 reaction systems in these experiments, only the signal of the H-loss channel was identified because high noise levels originating from fragmentation of the parent C_4H_8 ion made it unfeasible to reliably detect loss channels of larger radicals (e.g., the methyl loss). The translational energy flux distribution $P(E_T)$ and center-of-mass angular distribution $T(\theta)$ obtained for the C + C_4H_8 reactions confirm that the reaction channel leading to all the RSFR products, as inferred from the combined experimental and theoretical data, involves indirect scattering dynamics through the formation of one or more C_5H_8 intermediates.

The branching ratios, derived from RRKM calculations, are highly sensitive to the alkene structure. For *cis*- and *trans*-2-butene, the entropically favored β-scission channel (CH_3 loss) in the triplet 1,3-dimethylallene isomers dominates, affording 1-methylpropargyl (**p1**) with branching ratios of 80−90%, while the H atom loss channel produces 1,3-dimethylpropargyl (**p2**) with ≈10−20%; the formation of **p2** is supported by the agreement between the measured and calculated reaction energetics. For isobutene, methyl and hydrogen losses compete nearly equally: methyl loss from triplet 1,1-dimethylallene yields 3-methylpropargyl (**p5**) with a branching ratio marginally above 50%, whereas H atom loss from the same intermediate affords 1,1-dimethylpropargyl (**p6**) with slightly more than 40%; the product, which is assigned to 2-vinylallyl (**p7**) based on the consistency of the experimental energy release with the theoretical prediction, formed via a minor channel. In contrast, 1-butene stands out as the only isomer where a single hydrogen shift (**i18** → **i19**) redirects the entire reaction course. Here, the H atom loss channel prevails, leading to the product 1-vinylallyl (**p3**), whose experimental identification was deduced from the comparison of the experimental translational energy release with the calculated exothermicity. This product is formed via **i16** → **i17** → **i18** → **i19** → **p3** channel with a relative yield of 37.5% at the experimental collision energy, rising to 50% in the zero-collision-energy limit. The second significant channel is ethyl loss from triplet 1-ethylallene, affording propargyl (**p9**) with up to 26%. The combined contribution of propargyl-family radicals (**p9**, **p11**, **p14**) reaches ≈40%, slightly outweighing the allyl-type product **p3**.

These findings are potentially relevant not only for cold molecular clouds, where atomic carbon remains highly reactive under conditions of limited thermal activation, but also for oxygen-deficient environments, such as the circumstellar envelope of the carbon-rich star IRC+10216, where oxidation of the newly formed RSFRs is expected to play a negligible role.[97] In such regions, RSFRs could accumulate, and their subsequent radical−radical recombination may serve as a driver for molecular mass growth toward polycyclic aromatic hydrocarbons and their alkylated derivatives. Once these RSFRs and their alkylated counterparts are formed, for instance, via reactions of atomic carbon with the simplest C_2−C_4 alkenes, they become key building blocks for further carbonaceous growth. The present work expands the known chemistry of propargyl-type RSFRs, but the broader picture also includes allyl-type radicals with their alkyl or even alkenyl-substituted congeners, such as the 1- and 2-vinylallyl radicals (**p3** and **p7**) obtained in our reaction systems. Indeed, the recombination of propargyl and allyl and the self-recombination of allyl radicals[98,99] represent an alternative pathway of molecular growth processes in combustion and interstellar environments. The actual abundance and lifetime of these specific alkylated RSFRs in cold molecular clouds depend on a multitude of factors not considered here, but the present work identifies a potential low-temperature formation route.

■ ASSOCIATED CONTENT

Supporting Information

The Supporting Information is available free of charge at https://pubs.acs.org/doi/10.1021/acs.jpca.6c02765.

TOF spectra at m/z = 66 and 67 for all the C + C_4H_8 systems (Figure S1), alternative reaction pathways for C + isobutene and C + 1-butene reactions, full PES (Figures S2−S7), RRKM rate constants (Tables S1−S4), optimized Cartesian coordinates and vibrational frequencies for all reactants, intermediates, transition states, and products involved in the C + C_4H_8 reactions at the ωB97X-D/6-311G(d,p) level (PDF)

■ AUTHOR INFORMATION

Corresponding Authors

Alexander M. Mebel − *Department of Chemistry and Biochemistry, Florida International University, Miami 33199 Florida, United States;* orcid.org/0000-0002-7233-3133; Email: mebela@fiu.edu

Ralf I. Kaiser − *Department of Chemistry, University of Hawai'i at Manoa, Honolulu 96822 Hawaii, United States;* orcid.org/0000-0002-7233-7206; Email: ralfk@hawaii.edu

Authors

Anatoliy A. Nikolayev − *Samara National Research University, Samara 443086, Russia;* orcid.org/0000-0002-1733-3704

Iakov A. Medvedkov − *Department of Chemistry, University of Hawai'i at Manoa, Honolulu 96822 Hawaii, United States;* orcid.org/0000-0003-0672-2090

Surajit Metya − *Department of Chemistry, University of Hawai'i at Manoa, Honolulu 96822 Hawaii, United States;* orcid.org/0009-0004-5583-8481

Shane J. Goettl − *Department of Chemistry, University of Hawai'i at Manoa, Honolulu 96822 Hawaii, United States;* orcid.org/0000-0003-1796-5725

Complete contact information is available at: https://pubs.acs.org/10.1021/acs.jpca.6c02765

Author Contributions

The manuscript was written through contributions of all authors. All authors have given approval to the final version of the manuscript.

Notes

The authors declare no competing financial interest.

■ ACKNOWLEDGMENTS

The experimental studies at the University of Hawai'i were supported by the US Department of Energy, Basic Energy Sciences DE-FG02-03ER15411.

■ REFERENCES

(1) Keene, J.; Young, K.; Phillips, T. G.; Buettgenbach, T. H.; Carlstrom, J. E. Atomic Carbon in the Envelope of IRC+10216. *Astrophys. J., Lett.* **1993**, *415*, L131−L134.
(2) Van der Veen, W. E. C. J.; Huggins, P. J.; Matthews, H. E. Atomic carbon in the circumstellar envelopes of evolved stars. *Astrophys. J.* **1998**, *505* (2), 749−755.
(3) Ingalls, J. G.; Chamberlin, R. A.; Bania, T. M.; Jackson, J. M.; Lane, A. P.; Stark, A. A. Atomic carbon in southern hemisphere high-latitude clouds. *Astrophys. J.* **1997**, *479* (1), 296−302.
(4) Wilson, C. D. Atomic carbon emission from individual molecular clouds in M33. *Astrophys. J., Lett.* **1997**, *487* (1), L49−L52.
(5) Young, K. Neutral carbon in the protoplanetary nebulae CRL 618 and CRL 2688. *Astrophys. J., Lett.* **1997**, *488* (2), L157−L160.
(6) Sofia, U. J.; Cardelli, J. A.; Guerin, K. P.; Meyer, D. M. Carbon in the diffuse interstellar medium. *Astrophys. J., Lett.* **1997**, *482* (1), L105−L108.
(7) White, G. J.; Sandell, G. C. I. CO and 790 μm continuum observations of the Orion molecular cloud and ionisation bar. *Astron. Astrophys.* **1995**, *299*, 179−192.
(8) Yang, Z.; Galimova, G. R.; He, C.; Goettl, S. J.; Li, X.; Mebel, A. M.; Kaiser, R. I. An Unconventional Dark Radical Chemistry in Dense Molecular Clouds: Directed Gas-Phase Formation of Naphthyl Radicals. *J. Am. Chem. Soc.* **2025**, *147* (51), 47359−47369.
(9) Yang, Z.; Galimova, G. R.; He, C.; Goettl, S. J.; Paul, D.; Lu, W.; Ahmed, M.; Mebel, A. M.; Li, X.; Kaiser, R. I. Gas-phase formation of the resonantly stabilized 1-indenyl ($C_9H_7\bullet$) radical in the interstellar medium. *Sci. Adv.* **2023**, *9* (36), No. eadi5060.
(10) Wilson, A. V.; Parker, D. S.; Zhang, F.; Kaiser, R. I. Crossed beam study of the atom-radical reaction of ground state carbon atoms ($C(^3P)$) with the vinyl radical ($C_2H_3(X^2A')$). *Phys. Chem. Chem. Phys.* **2012**, *14* (2), 477−481.
(11) Parker, D. S.; Zhang, F.; Kim, Y. S.; Kaiser, R. I.; Mebel, A. M. On the Formation of Resonantly Stabilized C_5H_3 Radicals: A Crossed Beam and Ab Initio Study of the Reaction of Ground State Carbon Atoms with Vinylacetylene. *J. Phys. Chem. A* **2011**, *115* (5), 593−601.
(12) Sun, B. J.; Huang, C. H.; Tsai, M. F.; Sun, H. L.; Gao, L. G.; Wang, Y. S.; Yeh, Y. Y.; Shih, Y. H.; Sia, Z. F.; Chen, P. H.; Kaiser, R. I.; Chang, A. H. H. Synthesis of interstellar 1,3,5-heptatriynylidyne, C_7H, via the neutral-neutral reaction of ground state carbon atom, C, with triacetylene, HC_6H. *J. Chem. Phys.* **2009**, *131* (10), 104305.
(13) Kaiser, R. I.; Mebel, A. M. The reactivity of ground-state carbon atoms with unsaturated hydrocarbons in combustion flames and in the interstellar medium. *Int. Rev. Phys. Chem.* **2002**, *21* (2), 307−356.
(14) Hahndorf, I.; Lee, Y. T.; Kaiser, R. I.; Vereecken, L.; Peeters, J.; Bettinger, H. F.; Schreiner, P. R.; Schleyer, P. v. R.; Allen, W. D.; Schaefer, H. F., III A combined crossed-beam, ab initio, and Rice−Ramsperger−Kassel−Marcus investigation of the reaction of carbon atoms $C(^3P_j)$ with benzene, $C_6H_6(X^1A_{1g})$ and d_6-benzene, $C_6D_6(X^1A_{1g})$. *J. Chem. Phys.* **2002**, *116* (8), 3248−3262.
(15) Balucani, N.; Lee, H. Y.; Mebel, A. M.; Lee, Y. T.; Kaiser, R. I. A combined crossed beam and ab initio investigation on the reaction of carbon species with C_4H_6 isomers. III. 1,2-butadiene, $H_2CCCH-(CH_3)$ (X^1A') - a non-Rice-Ramsperger-Kassel-Marcus system? *J. Chem. Phys.* **2001**, *115*, 5107−5116.
(16) Huang, L. C. L.; Lee, H. Y.; Mebel, A. M.; Lin, S. H.; Lee, Y. T.; Kaiser, R. I. A combined crossed beam and ab initio investigation on the reaction of carbon species with C_4H_6 isomers. II. The dimethylacetylene molecule, H_3CCCCH_3 (X^1A_{1g}). *J. Chem. Phys.* **2000**, *113*, 9637−9648.
(17) Hahndorf, I.; Lee, H. Y.; Mebel, A. M.; Lin, S. H.; Lee, Y. T.; Kaiser, R. I. A Combined Crossed Beam and Ab Initio Investigation on the Reaction of Carbon Species with C_4H_6 Isomers. I. The 1,3-Butadiene Molecule. *J. Chem. Phys.* **2000**, *113*, 9622−9636.
(18) Miller, J. A.; Klippenstein, S. J. The recombination of propargyl radicals: Solving the master equation. *J. Phys. Chem. A* **2001**, *105* (30), 7254−7266.
(19) Miller, J. A.; Klippenstein, S. J. The recombination of propargyl radicals and other reactions on a C_6H_6 potential. *J. Phys. Chem. A* **2003**, *107* (39), 7783−7799.
(20) Klippenstein, S. J.; Miller, J. A.; Jasper, A. W. Kinetics of propargyl radical dissociation. *J. Phys. Chem. A* **2015**, *119* (28), 7780−7791.
(21) Mebel, A. M.; Kaiser, R. I. Formation of resonantly stabilised free radicals via the reactions of atomic carbon, dicarbon, and tricarbon with unsaturated hydrocarbons: theory and crossed molecular beams experiments. *Int. Rev. Phys. Chem.* **2015**, *34* (4), 461−514.
(22) Zhao, L.; Lu, W.; Ahmed, M.; Zagidullin, M. V.; Azyazov, V. N.; Morozov, A. N.; Mebel, A. M.; Kaiser, R. I. Gas-phase synthesis of benzene via the propargyl radical self-reaction. *Sci. Adv.* **2021**, *7*, No. eabf0360.
(23) Mebel, A. M.; Agúndez, M.; Cernicharo, J.; Kaiser, R. I. Elucidating the Formation of Ethynylbutatrienylidene (HCCCHCCC; X^1A') in the Taurus Molecular Cloud (TMC-1) via the Gas-Phase Reaction of Tricarbon (C_3) with the Propargyl Radical (C_3H_3). *Astrophys. J., Lett.* **2023**, *945*, L40.
(24) He, C.; Kaiser, R. I.; Lu, W.; Ahmed, M.; Krasnoukhov, V. S.; Pivovarov, P. S.; Zagidullin, M. V.; Azyazov, V. N.; Morozov, A. N.; Mebel, A. M. Unconventional gas-phase preparation of the prototype polycyclic aromatic hydrocarbon naphthalene ($C_{10}H_8$) via the reaction of benzyl (C_7H_7) and propargyl (C_3H_3) radicals coupled with hydrogen-atom assisted isomerization. *Chem. Sci.* **2023**, *14* (20), 5369−5378.
(25) Wang, C. Y.; Zhao, L.; Kaiser, R. I. Gas-Phase Preparation of the 14π Hückel Polycyclic Aromatic Anthracene and Phenanthrene Isomers ($C_{14}H_{10}$) via the Propargyl Addition−BenzAnnulation (PABA) Mechanism. *ChemPhysChem* **2024**, *25* (14), No. e202400151.
(26) Goettl, S. J.; Ahmed, M.; Mebel, A. M.; Kaiser, R. I. Molecular Mass Growth Processes to Polycyclic Aromatic Hydrocarbons through Radical−Radical Reactions Exploiting Photoionization Reflectron Time-of-Flight Mass Spectrometry. *Acc. Chem. Res.* **2025**, *58* (17), 2682−2694.
(27) Gao, J.; Li, Y.; Shang, Y.; Liu, Y.; Liu, B.; Guan, J.; Wang, Z.; Hu, Y. Propargyl ($\bullet C_3H_3$) and butadienyl ($\bullet i$-C_4H_5) radical−radical reactions well-skipping to vinylcyclopentadienyl radical and toluene: A theoretical and kinetic modeling study. *J. Chem. Phys.* **2025**, *163* (9), 094303.
(28) Klippenstein, S. J.; Kohse-Höinghaus, K. Combustion in a sustainable world: from molecules to processes. *J. Phys. Chem. A* **2023**, *127* (17), 3737−3742.
(29) Reizer, E.; Viskolcz, B.; Fiser, B. Formation and growth mechanisms of polycyclic aromatic hydrocarbons: A mini-review. *Chemosphere* **2022**, *291*, 132793.
(30) Thomas, A. M.; He, C.; Zhao, L.; Galimova, G. R.; Mebel, A. M.; Kaiser, R. I. Combined experimental and computational study on the reaction dynamics of the 1-propynyl (CH_3CC)−1,3-butadiene ($CH_2CHCHCH_2$) system and the formation of toluene under single collision conditions. *J. Phys. Chem. A* **2019**, *123* (19), 4104−4118.
(31) Matsugi, A.; Miyoshi, A. Modeling of two- and three-ring aromatics formation in the pyrolysis of toluene. *Proc. Combust. Inst.* **2013**, *34* (1), 269−277.
(32) Hansen, N.; Cool, T. A.; Westmoreland, P. R.; Kohse-Höinghaus, K. Recent contributions of flame-sampling molecular-beam mass spectrometry to a fundamental understanding of combustion chemistry. *Prog. Energy Combust. Sci.* **2009**, *35* (2), 168−191.

https://doi.org/10.1021/acs.jpca.6c02765
J. Phys. Chem. A 2026, 130, 4823−4838

(33) Medvedkov, I. A.; Nikolayev, A. A.; He, C.; Yang, Z.; Mebel, A. M.; Kaiser, R. I. One Collision—Two Substituents: Gas-Phase Preparation of Xylenes under Single-Collision Conditions. *Angew. Chem., Int. Ed.* **2024**, *63*, No. e202315147.
(34) Galimova, G. R.; Medvedkov, I. A.; Mebel, A. M. The role of methylaryl radicals in the growth of polycyclic aromatic hydrocarbons: The formation of five-membered rings. *J. Phys. Chem. A* **2022**, *126* (7), 1233−1244.
(35) Peña, G. D. G.; Alrefaai, M. M.; Yang, S. Y.; Raj, A.; Brito, J. L.; Stephen, S.; Anjana, T.; Pillai, V.; Al Shoaibi, A.; Chung, S. H. Effects of methyl group on aromatic hydrocarbons on the nanostructures and oxidative reactivity of combustion-generated soot. *Combust. Flame* **2016**, *172*, 1−12.
(36) Sephton, M. A. in *Treatise on Geochemistry* (Elsevier, Amsterdam, 2014). pp 1−31.
(37) Sephton, M. A. Aromatic units from the macromolecular material in meteorites: Molecular probes of cosmic environments. *Geochim. Cosmochim. Acta* **2013**, *107*, 231−241.
(38) Matsugi, A.; Miyoshi, A. Kinetics of the self-reactions of benzyl and o-xylyl radicals studied by cavity ring-down spectroscopy. *Chem. Phys. Lett.* **2012**, *521*, 26−30.
(39) da Silva, G.; Moore, E. E.; Bozzelli, J. W. Decomposition of methylbenzyl radicals in the pyrolysis and oxidation of xylenes. *J. Phys. Chem. A* **2009**, *113* (38), 10264−10278.
(40) Medvedkov, I. A.; Nikolayev, A. A.; Yang, Z.; Goettl, S. J.; Mebel, A. M.; Kaiser, R. I. Elucidating the chemical dynamics of the elementary reactions of the 1-propynyl radical (CH_3CC; X^2A_1) with 2-methylpropene ($(CH_3)_2CCH_2$; X^1A_1). *Phys. Chem. Chem. Phys.* **2024**, *26* (7), 6448−6457.
(41) Medvedkov, I. A.; Nikolayev, A. A.; He, C.; Yang, Z.; Mebel, A. M.; Kaiser, R. I. A combined experimental and computational study on the reaction dynamics of the 1-propynyl (CH_3CC, X^2A_1)−propylene (CH_3CHCH_2, X^1A') system: formation of 1,3-dimethylvinylacetylene ($CH_3CCCHCHCH_3$, X^1A') under single collision conditions. *Mol. Phys.* **2024**, *122* (7−8), No. e2234509.
(42) Goettl, S. J.; Medvedkov, I. A.; Nikolayev, A. A.; He, C.; Yang, Z.; Mebel, A. M.; Somani, A.; Portela-Gonzalez, A.; Sander, W.; Kaiser, R. I. Gas-Phase Synthesis of Naphthalene Through an Unconventional Thermal Alkyne-Alkene [2 + 2] Cycloaddition Mechanism. *Chem. Sci.* **2025**, *16*, 22621−22629.
(43) Goettl, S. J.; Yang, Z.; He, C.; Somani, A.; Portela-Gonzalez, A.; Sander, W.; Mebel, A. M.; Kaiser, R. I. Exploring the Chemical Dynamics of Phenanthrene ($C_{14}H_{10}$) Formation via the Bimolecular Gas-Phase Reaction of the Phenylethynyl Radical (C_6H_5CC) with Benzene (C_6H_6). *Faraday Discuss.* **2024**, *251*, 509−522.
(44) Goettl, S. J.; Yang, Z.; Kollotzek, S.; Paul, D.; Kaiser, R. I.; Somani, A.; Portela-Gonzalez, A.; Sander, W.; Nikolayev, A. A.; Azyazov, V. N.; Mebel, A. M. Exploring the Chemical Dynamics of Phenylethynyl Radical (C_6H_5CC; X^2A_1) Reactions with Allene (H_2CCCH_2; X^1A_1) and Methylacetylene (CH_3CCH; X^1A_1). *J. Phys. Chem. A* **2023**, *127*, 5723−5733.
(45) Becker, L.; Bunch, T. E. Fullerenes, fulleranes and polycyclic aromatic hydrocarbons in the Allende meteorite. *Meteorit. Planet. Sci.* **1997**, *32* (4), 479−487.
(46) Hayatsu, R.; Matsuoka, S.; Scott, R. G.; Studier, M. H.; Anders, E. Origin of organic matter in the early solar system—VII. The organic polymer in carbonaceous chondrites. *Geochim. Cosmochim. Acta* **1977**, *41* (9), 1325−1339.
(47) Greenberg, J. M.; Mendoza-Gómez, C. X.; Pirronello, V. *The Chemistry of Life's Origins*; Springer Science & Business Media, 2012; Vol. *416*, pp 209−258.
(48) Hayes, J. M. Organic constituents of meteorites—a review. *Geochim. Cosmochim. Acta* **1967**, *31* (9), 1395−1440.
(49) Callahan, M. P.; Abo-Riziq, A.; Crews, B.; Grace, L.; de Vries, M. S. Isomer discrimination of polycyclic aromatic hydrocarbons in the Murchison meteorite by resonant ionization. *Spectrochim. Acta, Part A* **2008**, *71* (4), 1492−1495.
(50) Lecasble, M.; Remusat, L.; Viennet, J. C.; Laurent, B.; Bernard, S. Polycyclic aromatic hydrocarbons in carbonaceous chondrites can be used as tracers of both pre-accretion and secondary processes. *Geochim. Cosmochim. Acta* **2022**, *335*, 243−255.
(51) Kalpana, M. S.; Babu, E. V. S. S. K.; Mani, D.; Tripathi, R. P.; Bhandari, N. Polycyclic aromatic hydrocarbons in the Mukundpura (CM2) Chondrite. Planet. *Space Sci.* **2021**, *198*, 105177.
(52) Aponte, J. C.; Dworkin, J. P.; Glavin, D. P.; Elsila, J. E.; Parker, E. T.; McLain, H. L.; Naraoka, H.; Okazaki, R.; Takano, Y.; Tachibana, S.; Dong, G.; Zeichner, S. S.; Eiler, J. M.; Yurimoto, H.; Nakamura, T.; Yabuta, H.; Terui, F.; Noguchi, T.; Sakamoto, K.; Yada, T.; Nishimura, M.; Nakato, A.; Miyazaki, A.; Yogata, K.; Abe, M.; Okada, T.; Usui, T.; Yoshikawa, M.; Saiki, T.; Tanaka, S.; Nakazawa, S.; Tsuda, Y.; Watanabe, S. Hayabusa2-initial-analysis SOM team; Hayabusa2-initial-analysis core team. PAHs, hydrocarbons, and dimethylsulfides in Asteroid Ryugu samples A0106 and C0107 and the Orgueil (CI1) meteorite. *Earth, Planets Space* **2023**, *75* (1), 28.
(53) Xue, X. S.; Ji, P.; Zhou, B.; Cheng, J. P. The essential role of bond energetics in C−H activation/functionalization. *Chem. Rev.* **2017**, *117* (13), 8622−8648.
(54) Li, S. H.; Guo, J. J.; Li, R.; Wang, F.; Li, X. Y. Theoretical prediction of rate constants for hydrogen abstraction by OH, H, O, CH_3, and HO_2 radicals from toluene. *J. Phys. Chem. A* **2016**, *120* (20), 3424−3432.
(55) Kislov, V. V.; Mebel, A. M. Ab initio G3-type/statistical theory study of the formation of indene in combustion flames. I. Pathways involving benzene and phenyl radical. *J. Phys. Chem. A* **2007**, *111* (19), 3922−3931.
(56) Oehlschlaeger, M. A.; Davidson, D. F.; Hanson, R. K. Experimental investigation of toluene + H → benzyl + H_2 at high temperatures. *J. Phys. Chem. A* **2006**, *110* (32), 9867−9873.
(57) Fröchtenicht, R. The photodissociation of toluene studied by forward photofragment translational spectroscopy. *J. Chem. Phys.* **1995**, *102* (12), 4850−4859.
(58) McGuire, B. A. census of interstellar, circumstellar, extragalactic, protoplanetary disk, and exoplanetary molecules. Astrophys. *J. Suppl. Ser.* **2022**, *259* (2), 30.
(59) Kaiser, R. I.; Balucani, N.; Charkin, D. O.; Mebel, A. M. A crossed beam and ab initio study of the $C_2(X^1\Sigma_g^+/a^3\Pi_u)$ + $C_2H_2(X^1\Sigma_g^+)$ reactions. *Chem. Phys. Lett.* **2003**, *382* (1−2), 112−119.
(60) Kaiser, R. I.; Mebel, A. M.; Chang, A. H. H.; Lin, S. H.; Lee, Y. T. Crossed-beam reaction of carbon atoms with hydrocarbon molecules. V. Chemical dynamics of *n*-C_4H_3 formation from reaction of $C(^3P_j)$ with allene, $H_2CCCH_2(X^1A_1)$. *J. Chem. Phys.* **1999**, *110* (21), 10330−10344.
(61) Chin, C. H.; Chen, W. K.; Huang, W. J.; Lin, Y. C.; Lee, S. H. Exploring the dynamics of reaction $C(^3P)$ + C_2H_4 with crossed beam/photoionization experiments and quantum chemical calculations. *J. Phys. Chem. A* **2012**, *116* (29), 7615−7622.
(62) Chastaing, D.; James, P. L.; Sims, I. R.; Smith, I. W. Neutral−neutral reactions at the temperatures of interstellar clouds: Rate coefficients for reactions of atomic carbon, $C(^3P)$, with O_2, C_2H_2, C_2H_4 and C_3H_6 down to 15 K. *Phys. Chem. Chem. Phys.* **1999**, *1* (9), 2247−2256.
(63) Kaiser, R. I.; Lee, Y. T.; Suits, A. G. Crossed-beam reaction of carbon atoms with hydrocarbon molecules. I. Chemical dynamics of the propargyl radical formation, C_3H_3 (X^2B_2), from reaction of $C(^3P_j)$ with ethylene, C_2H_4 (X^1A_g). *J. Chem. Phys.* **1996**, *105* (19), 8705−8720.
(64) Le, T. N.; Lee, H. Y.; Mebel, A. M.; Kaiser, R. I. Ab initio MO study of the triplet C_3H_4 potential energy surface and the reaction of $C(^3P_j)$ with ethylene. *C2H4. J. Phys. Chem. A* **2001**, *105* (10), 1847−1856.
(65) Naulin, C.; Daugey, N.; Hickson, K. M.; Costes, M. Dynamics of the Reactions of $C(^3P_j)$ Atoms with Ethylene, Allene, and Methylacetylene at Low Energy Revealed by Doppler−Fizeau Spectroscopy. *J. Phys. Chem. A* **2009**, *113* (52), 14447−14457.
(66) Lee, S. H.; Chen, W. K.; Chin, C. H.; Huang, W. J. Dynamics of carbon-hydrogen and carbon-methyl exchanges in the collision of ^3P atomic carbon with propene. *J. Chem. Phys.* **2013**, *139* (17), 174317.

https://doi.org/10.1021/acs.jpca.6c02765
J. Phys. Chem. A 2026, 130, 4823−4838

(67) Chin, C. H.; Chen, W. K.; Huang, W. J.; Lin, Y. C.; Lee, S. H. Identification of C_4H_5, C_4H_4, C_3H_3 and CH_3 radicals produced from the reaction of atomic carbon with propene: Implications for the atmospheres of Titan and giant planets and for the interstellar medium. *Icarus* **2013**, *222* (1), 254−262.
(68) Bourgalais, J.; Spencer, M.; Osborn, D. L.; Goulay, F.; Le Picard, S. D. Reactions of atomic carbon with butene isomers: Implications for molecular growth in carbon-rich environments. *J. Phys. Chem. A* **2016**, *120* (46), 9138−9150.
(69) Kaiser, R. I.; Maksyutenko, P.; Ennis, C.; Zhang, F.; Gu, X.; Krishtal, S. P.; Mebel, A. M.; Kostko, O.; Ahmed, M. Untangling the chemical evolution of Titan's atmosphere and surface − from homogeneous to heterogeneous chemistry. *Faraday Discuss.* **2010**, *147*, 429−478.
(70) Guo, Y.; Gu, X.; Kawamura, E.; Kaiser, R. I. Design of a modular and versatile interlock system for ultrahigh vacuum machines: A crossed molecular beam setup as a case study. *Rev. Sci. Instrum.* **2006**, *77* (3), 034701.
(71) Gu, X.; Guo, Y.; Mebel, A. M.; Kaiser, R. I. A crossed beam investigation of the reactions of tricarbon molecules, $C_3(X^1\Sigma_g^+)$, with acetylene, $C_2H_2(X^1\Sigma_g^+)$, ethylene, $C_2H_4(X^1A_g)$, and benzene, $C_6H_6(X^1A_{1g})$. *Chem. Phys. Lett.* **2007**, *449* (1−3), 44−52.
(72) Gu, X.; Guo, Y.; Kawamura, E.; Kaiser, R. I. Characteristics and diagnostics of an ultrahigh vacuum compatible laser ablation source for crossed molecular beam experiments. *J. Vac. Sci. Technol., A* **2006**, *24* (3), 505−511.
(73) Medvedkov, I. A.; Nikolayev, A. A.; Goettl, S. J.; Yang, Z.; Mebel, A. M.; Kaiser, R. I. Experimental and theoretical study of the Sn−O bond formation between atomic tin and molecular oxygen. *Phys. Chem. Chem. Phys.* **2024**, *26* (43), 27763−27771.
(74) Daly, N. R. Scintillation type mass spectrometer ion detector. *Rev. Sci. Instrum.* **1960**, *31* (3), 264−267.
(75) Lee, Y. T. Molecular beam studies of elementary chemical processes. *Science* **1987**, *236* (4803), 793−798.
(76) Herschbach, D. R. Molecular dynamics of elementary chemical reactions (Nobel Lecture). *Angew. Chem., Int. Ed. Engl.* **1987**, *26* (12), 1221−1243.
(77) Vernon, M. F. Molecular Beam Scattering; University of California: Berkeley, 1983, Ph.D. Dissertation.
(78) Weiss, P. S.; Mestdagh, J. M.; Schmidt, H.; Vernon, M. F.; Covinsky, M. H.; Balko, B. A.; Lee, Y. T. Reaction dynamics of electronically excited alkali atoms with simple molecules. *J. Chin. Chem. Soc.* **1985**, *32* (3), 179−185.
(79) Levine, R. D. *Molecular Reaction Dynamics*; Cambridge University Press: Cambridge, UK, 2009.
(80) Steinfeld, J. I.; Francisco, J. S.; Hase, W. L. *Chemical Kinetics and Dynamics*, 2 ed.; Pearson: Upper Saddle River, NJ, 1998.
(81) Chai, J.-D.; Head-Gordon, M. Long-Range Corrected Hybrid Density Functionals with Damped Atom−Atom Dispersion Corrections. *Phys. Chem. Chem. Phys.* **2008**, *10* (44), 6615−6620.
(82) Krishnan, R.; Binkley, J. S.; Seeger, R.; Pople, J. A. Self Consistent Molecular Orbital Methods. XX. A Basis Set for Correlated Wave Functions. *J. Chem. Phys.* **1980**, *72* (1), 650−654.
(83) Frisch, M. J.; Trucks, G. W.; Schlegel, H. B.; Scuseria, G. E.; Robb, M. A.; Cheeseman, J. R.; Scalmani, G.; Barone, V.; Petersson, G. A.; Nakatsuji, H.; Li, X.; Caricato, M.; Marenich, A. V.; Bloino, J.; Janesko, B. G.; Gomperts, R.; Mennucci, B.; Hratchian, H. P.; Ortiz, J. V.; Izmaylov, A. F.; Sonnenberg, J. L.; Williams; Ding, F.; Lipparini, F.; Egidi, F.; Goings, J.; Peng, B.; Petrone, A.; Henderson, T.; Ranasinghe, D.; Zakrzewski, V. G.; Gao, J.; Rega, N.; Zheng, G.; Liang, W.; Hada, M.; Ehara, M.; Toyota, K.; Fukuda, R.; Hasegawa, J.; Ishida, M.; Nakajima, T.; Honda, Y.; Kitao, O.; Nakai, H.; Vreven, T.; Throssell, K.; Montgomery, J. A., Jr.; Peralta, J. E.; Ogliaro, F.; Bearpark, M. J.; Heyd, J. J.; Brothers, E. N.; Kudin, K. N.; Staroverov, V. N.; Keith, T. A.; Kobayashi, R.; Normand, J.; Raghavachari, K.; Rendell, A. P.; Burant, J. C.; Iyengar, S. S.; Tomasi, J.; Cossi, M.; Millam, J. M.; Klene, M.; Adamo, C.; Cammi, R.; Ochterski, J. W.; Martin, R. L.; Morokuma, K.; Farkas, O.; Foresman, J. B.; Fox, D. J. *Gaussian 09, Revision A.02*; Gaussian, Inc.: Wallingford, CT, 2016.
(84) Hratchian, H. P.; Schlegel, H. B. Accurate Reaction Paths Using a Hessian Based Predictor−Corrector Integrator. *J. Chem. Phys.* **2004**, *120* (21), 9918−9924.
(85) Werner, H.-J.; Knowles, P. J.; Lindh, R.; Manby, F. R.; Schütz, M.; Celani, P.; Korona, T.; Rauhut, G.; Amos, R. D.; Bernhardsson, A. *MOLPRO, Revision 2015.1, A Package of Ab Initio Programs*; University of: Cardiff: Cardiff, UK, 2015.
(86) Adler, T. B.; Knizia, G.; Werner, H.-J. A Simple and Efficient CCSD(T)-F12 Approximation. *J. Chem. Phys.* **2007**, *127* (22), 221106.
(87) Knizia, G.; Adler, T. B.; Werner, H.-J. Simplified CCSD(T)-F12 Methods: Theory and Benchmarks. *J. Chem. Phys.* **2009**, *130* (5), 054104.
(88) Dunning, T. H., Jr Gaussian Basis Sets for Use in Correlated Molecular Calculations. I. The Atoms Boron through Neon and Hydrogen. *J. Chem. Phys.* **1989**, *90* (2), 1007−1023.
(89) Zhang, J.; Valeev, E. F. Prediction of reaction barriers and thermochemical properties with explicitly correlated coupled-cluster methods: A basis set assessment. *J. Chem. Theory Comput.* **2012**, *8* (9), 3175−3186.
(90) Robinson, P. J.; Holbrook, K. A. *Unimolecular Reactions*; John Wiley and Sons: New York, 1972.
(91) Eyring, H.; Lin, S. H.; Lin, S. M. *Basic Chemical Kinetics*; John Wiley and Sons: New York, 1980.
(92) Kislov, V. V.; Nguyen, T. L.; Mebel, A. M.; Lin, S. H.; Smith, S. C. Photodissociation of Benzene under Collision-Free Conditions: An Ab Initio/Rice−Ramsperger−Kassel−Marcus Study. *J. Chem. Phys.* **2004**, *120* (15), 7008−7017.
(93) He, C.; Zhao, L.; Thomas, A. M.; Morozov, A. N.; Mebel, A. M.; Kaiser, R. I. Elucidating the Chemical Dynamics of the Elementary Reactions of the 1-Propynyl Radical (CH_3CC; X^2A_1) with Methylacetylene (H_3CCCH; X^1A_1) and Allene (H_2CCCH_2; X^1A_1). *J. Phys. Chem. A* **2019**, *123* (26), 5446−5462.
(94) Kaiser, R. I. Experimental investigation on the formation of carbon-bearing molecules in the interstellar medium via neutral−neutral reactions. *Chem. Rev.* **2002**, *102* (5), 1309−1358.
(95) Kaiser, R. I.; Mebel, A. M. On the formation of polyacetylenes and cyanopolyacetylenes in Titan's atmosphere and their role in astrobiology. *Chem. Soc. Rev.* **2012**, *41* (16), 5490−5501.
(96) Kaiser, R. I.; Ochsenfeld, C.; Stranges, D.; Head-Gordon, M.; Lee, Y. T. Combined Crossed Molecular Beams and Ab Initio Investigation of the Formation of Carbon-Bearing Molecules in the Interstellar Medium via Neutral−Neutral Reactions. *Faraday Discuss.* **1998**, *109* (0), 183−204.
(97) Agúndez, M.; Cernicharo, J. Oxygen chemistry in the circumstellar envelope of the carbon-rich star IRC+10216. *Astrophys. J.* **2006**, *650* (1), 374−393.
(98) Georgievskii, Y.; Miller, J. A.; Klippenstein, S. J. Association rate constants for reactions between resonance-stabilized radicals: C_3H_3 + C_3H_3, C_3H_3 + C_3H_5, and C_3H_5 + C_3H_5. *Phys. Chem. Chem. Phys.* **2007**, *9* (31), 4259−4268.
(99) Matsugi, A.; Suma, K.; Miyoshi, A. Kinetics and mechanisms of the allyl + allyl and allyl + propargyl recombination reactions. *J. Phys. Chem. A* **2011**, *115* (26), 7610−7624.

https://doi.org/10.1021/acs.jpca.6c02765
J. Phys. Chem. A 2026, 130, 4823−4838